

Implications of triangular features in the Gaia skymap for the Caustic Ring Model of the Milky Way halo

Sankha S. Chakrabarty^{a,b,c}, Yaqi Han^c, Anthony H. Gonzalez^d, and Pierre Sikivie^c

^a *Dipartimento di Fisica, Università di Torino, Via P. Giuria 1, I-10125 Torino, Italy*

^b *Istituto Nazionale di Fisica Nucleare (INFN), Sezione di Torino, Via P. Giuria 1, I-10125 Torino, Italy*

^c *Department of Physics, University of Florida, Gainesville, FL 32611, USA*

^d *Department of Astronomy, University of Florida, Gainesville, FL 32611, USA*

(Dated: June 8, 2021)

Abstract

The Gaia map of the Milky Way reveals a pair of triangular features at nearly symmetric locations on opposite sides of the Galactic Center. In this paper we explore the implications of these features assuming they are manifestations of a caustic ring in the dark matter distribution of the Milky Way halo. The existence of a series of such rings is predicted by the Caustic Ring Model. The model's phase-space distribution is that acquired by a rethermalizing Bose-Einstein condensate of axions or axion-like particles. We show that dust is gravitationally entrained by cold axion flows and propose this as an explanation for the sharpness of the triangular features. The locations of the features imply that we on Earth are much closer to the fifth caustic ring than thought on the basis of pre-Gaia observations. Most likely we are inside its tricusp cross-section. In that case the dark matter density on Earth is dominated by four cold flows, termed Big, Little, Up and Down. If we are outside the tricusp cross-section the dark matter density on Earth is dominated by two cold flows, Big and Little. We use the triangular features in the Gaia map, and a matching feature in the IRAS map, to estimate the velocity vectors and densities of the four locally dominant flows.

PACS numbers: 95.35.+d

I. INTRODUCTION

The identity of dark matter is widely regarded as one of the most central and important questions in science today. A related question is: what is the phase-space distribution of dark matter in galactic halos, and particularly what is the phase-space distribution of dark matter in the halo of our own Milky Way galaxy. This latter question is important for at least two reasons. First, the Milky Way halo is the environment in which the Galactic Disk forms and lights up with stars such as our Sun. Second, knowledge of the phase-space distribution helps direct and indirect dark matter searches on Earth. Finally, there is the tantalizing possibility that the phase-space distribution depends on the identity of the dark matter particle, and hence that observations of the phase-space distribution may reveal or constrain the dark matter’s identity.

Dark matter is generally thought to be cold and collisionless. “Cold” means that the primordial velocity dispersion of the dark matter particles is small, less than of order 10^{-8} today. Throughout, we use units in which $\hbar = c = k_B = 1$. “Collisionless” means that, to excellent approximation, gravity is the only relevant interaction among the dark matter particles as far as large scale structure formation is concerned. Particle candidates with these properties include weakly interacting massive particles (WIMPs), QCD axions or axion-like particles (ALPs), and sterile neutrinos [1].

Cold collisionless dark matter lies on a thin 3-dimensional hypersurface in 6-dimensional phase-space [2]. We refer to this 3-dimensional hypersurface as the phase-space sheet. Its qualitative behavior is described in Fig. 1. The thickness of the phase-space sheet is the primordial velocity dispersion. In the non-linear regime of structure formation, the phase-space sheet wraps around massive objects, such as galaxies, in phase-space. As a result, at any physical point inside a galactic halo there is an odd number flows. Furthermore, the dark matter density diverges in the limit of zero velocity dispersion on the surfaces in physical space across which the number of flows changes by two. Such surfaces are called caustics. The number of flows expected on Earth is of order one hundred [2]. Present N-body simulations have inadequate resolution for revealing any but a small number of the expected flows. Arguments for the robustness of cold flows and caustics in galactic halos are given in ref. [3].

The Caustic Ring Model is a proposal for the phase-space distribution of the dark matter halo of the Milky Way, and those of other disk galaxies [4]. The model is characterized by axial symmetry, self-similar time evolution, and large scale vorticity. Although real galaxies are not exactly axial symmetric, they are sufficiently so that the model may apply to them as a first approximation. According to the model, the inner caustics in the halos of disk galaxies are rings. Caustic rings are closed tubes whose cross-section is described by the elliptic umbilic (D_{-4}) catastrophe [5]. The cross-section has the shape of a tricuspid; see Fig. 2. The rings lie in the galactic plane. Their radii in any given disk galaxy are predicted in terms of a single adjustable parameter j_{\max} ; see Eq. (2.9). Observational evidence is claimed in support of the model.

Large scale vorticity is not possible if the dark matter is WIMPs or sterile neutrinos [6]. QCD axions [7, 8] and ALPs [9] produced by the vacuum realignment mechanism [10], including ultra-light ALPs, differ from WIMPs and sterile neutrinos in that they form a Bose-Einstein condensate [11–13]. Thermalization is a necessary condition for Bose-Einstein condensation. The interaction through which cold dark matter axions thermalize is self-gravity. When falling onto galactic halos, cold dark matter axions thermalize sufficiently

quickly that they almost all go to the lowest energy state available to them consistent with the total angular momentum they have acquired through tidal torquing [12, 14]. That state is one of rigid rotation in the angular variables. Thus axion (or ALP) dark matter does acquire vorticity in galactic halos, and accounts for the existence of caustic rings. It was shown that axion Bose-Einstein condensation accounts in fact for all properties of the Caustic Ring Model [15]. The observational evidence for caustic rings and the Caustic Ring Model is therefore evidence that the dark matter is a Bose-Einstein condensate, of axions or ALPs, at least in part.

The idea that the cold axion fluid thermalizes by gravitational self-interactions, and as a result forms a Bose-Einstein condensate, was criticized in refs. [16–18]. These criticisms were addressed in ref. [19].

One piece of evidence that has been claimed in support of caustic rings is a triangular feature in the IRAS map of the Milky Way plane; see <https://www.phys.ufl.edu/~sikivie/triangle/>. The triangular feature is interpreted as the imprint of the 5th caustic ring of dark matter in our galaxy upon baryonic matter in the Galactic Disk, seen in a direction tangent to the ring from our perspective [20]. The IRAS triangle is in the direction of Galactic Coordinates $(l, b) = (80^\circ, 0^\circ)$. The IRAS map does not have a matching triangular feature on the other side, near $(l, b) = (-80^\circ, 0^\circ)$. However, the recently released Gaia skymap [21, 22] has two triangular features. One of these coincides with the IRAS triangle on the left side. The other is on the right side, at $(l, b) = (-91^\circ, 0^\circ)$; see <https://www.phys.ufl.edu/~sikivie/Gaiamap/>. Our paper assumes the two features are effects of the 5th caustic ring on baryonic matter and explores the implications of this for the Caustic Ring Model. The fact that the two triangles do not match perfectly in direction is attributed to a displacement of the caustic ring center 5.8° towards the right relative to the Galactic Center.

Section III of our paper is concerned with the mechanism by which the caustic ring produces triangular features in the IRAS and Gaia maps. It was proposed in ref. [20] that the features are produced by gas and dust in thermal equilibrium in the gravitational field of the caustic ring. However, the features produced in this way have been found to be much less sharp than the observed features [23]. We propose here instead that dust is entrained by the cold axion flows forming the nearby caustic. Because the dust particles follow the same trajectories as the axions, they form the same caustics. This proposal accounts for the sharpness of the triangular features. We derive a formula for the drag on a dust particle moving with respect to a cold axion fluid and compare this to the drag on the dust particle as a result of collisions with gas in the disk. A major source of uncertainty is the temperature of the axions. We discuss the present axion temperature considering primordial heat in the axions themselves and heat absorbed later by cooling baryons.

When only the IRAS triangle was known, it was thought that the Sun lies close to, but outside of, the tricusp volume of the nearby caustic ring because it was assumed that the caustic ring center coincides with the Galactic Center. Now, taking account of the Gaia right triangle, the Sun is much closer to the caustic than previously thought. In fact we believe the Sun almost certainly is inside the tricusp volume of the 5th caustic ring. There are then four prominent flows on Earth associated with that caustic. Our goal in Section IV is to derive the properties of the four flows from the observed triangular features.

The outline of our paper is as follows. Section II describes caustic rings, the Caustic Ring Model and the observational evidence in support of it. The rotation curve of M31 and the Gaia triangles are presented as additional evidence. Section III discusses the entrainment

of dust by cold axion flows, and the effect of dust-gas and dust-dust collisions on the flow of dust. In Section IV, we use the IRAS and Gaia triangular features to determine the velocity vectors on Earth of the four flows associated with the nearby caustic ring. We also give rough estimates of their densities. Section V provides a summary.

II. THE CAUSTIC RING MODEL

The Caustic Ring Model is a proposal for the phase-space distribution of the halo of the Milky Way, and the halos of other disk galaxies. The model is axially symmetric, and self-similar in its time evolution. One of its distinguishing features is the presence of caustic rings of dark matter in the galactic plane. In this section we give background information on dark matter caustics, a detailed description of caustic rings, the model predictions for the caustic ring radii, and the previously claimed observational evidence in support of the model. Finally we present additional evidence from the rotation curve of M31 and from a couple of triangular features in the Gaia skymap.

A. Caustic rings

1. Dark matter caustics

Caustics appear in a flow of energy or matter when two conditions are satisfied: 1) the flow is collisionless and 2) the velocity dispersion of the flow is small. Cold dark matter particles are collisionless - i.e. they have only gravitational interactions in excellent approximation - and have very small primordial velocity dispersion δv [5, 6]. Hence, caustics are expected in the distribution of dark matter. They appear at the very moment multi-streaming begins. Indeed, as mentioned already in Section I, cold dark matter particles lie on a thin three-dimensional hypersurface embedded in six-dimensional phase-space. This phase-space sheet wraps around inhomogeneities such as galaxies. This results in a number of discrete flows through any point in physical space. Caustics lie at the boundaries of regions with differing number of flows, one region having K flows and the other $K + 2$ flows.

Each particle in the phase-space sheet can be labeled by three parameters $(\alpha_1, \alpha_2, \alpha_3) \equiv \vec{\alpha}$. Let $\vec{x}(\vec{\alpha}, t)$ be the position of particle $\vec{\alpha}$ at time t . The number K of discrete flows through a physical point \vec{r} is the number of solutions $\alpha_j(\vec{r}, t)$, $j = 1, 2, ..K$, of the equation $\vec{r} = \vec{x}(\vec{\alpha}, t)$. In physical space, the number density is given by

$$n(\vec{r}, t) = \sum_{j=1}^K \frac{1}{|D(\vec{\alpha}_j(\vec{r}, t), t)|} \frac{d^3 N}{d\alpha^3}(\vec{\alpha}_j(\vec{r}, t)) \quad (2.1)$$

where $\frac{d^3 N}{d\alpha^3}(\vec{\alpha})$ is the particle number density in parameter space, and $D(\vec{\alpha}, t) = \det\left(\frac{\partial \vec{x}}{\partial \vec{\alpha}}\right)$ is the Jacobian of the transformation $\vec{\alpha} \rightarrow \vec{x}(\vec{\alpha}, t)$. Eq. (2.1) shows that the physical space density diverges where the map $\vec{\alpha} \rightarrow \vec{x}(\vec{\alpha}, t)$ is singular.

2. Outer and inner caustics

Cold dark matter particles fall in and out of the gravitational potential well of a galaxy numerous times over the galaxy's history. The in and out flows of the particles necessarily form inner and outer caustics [5, 6]. The outer caustics are topological spheres. They appear near where the particles in an outflow are at their maximum distance from the galactic center before falling back in. The inner caustics appear near where the particles with the most angular momentum in an inflow are closest to the galactic center before falling back out. The structure of the inner caustics is determined by the velocity field of the particles at their last turnaround, i.e. when their radially outward flow was last stopped by the gravitational attraction of the galaxy. A shell containing such particles is called a turnaround sphere. When the velocity field is irrotational ($\vec{\nabla} \times \vec{v} = 0$), the inner caustics have a tent-like structure, described in ref. [6]. When the velocity field is dominated by net overall rotation ($\vec{\nabla} \times \vec{v} \neq 0$), the inner caustics are closed tubes with a *tricuspid* cross-section, called caustic rings. The structure of caustics is stable under small perturbations in the velocity field [6].

The inner caustics provide a tool to differentiate between a rethermalizing Bose-Einstein condensate of axions, or ALPs, and the other dark matter candidates. Ordinary CDM, including WIMPs and sterile neutrinos, never acquires a velocity field with large scale rotation. Indeed primordial rotational modes die out as a result of the Hubble expansion, setting $\vec{\nabla} \times \vec{v} = 0$ as an initial condition for all dark matter candidates. Galactic halos acquire angular momentum through tidal torquing by nearby protogalaxies in the early phases of structure formation [24]. Even though galactic halos acquire angular momentum, the velocity field of the dark matter particles remains irrotational if the dark matter is ordinary CDM [6]. The inner caustics have tent-like structure in that case. Axions, as well as any axion-like particles (ALPs) produced by the vacuum realignment mechanism [10], behave differently from ordinary CDM because they thermalize as a result of their gravitational self-interactions and form a Bose-Einstein condensate (BEC) [11–13]. Dark matter axions rethermalize sufficiently fast by gravitational self-interactions while they fall in and out of a galactic gravitational potential well that almost all go to the lowest energy available state consistent with the angular momentum acquired by tidal torquing [12, 14]. That state is one of rigid rotation on the turnaround sphere. As a result dark matter axions fall in with a rotational velocity field and make caustic rings. The observational evidence for caustic rings, discussed below, suggests therefore that the dark matter is axions, or ALPs, at least in part. If the dark matter is a mixture of axions and ordinary cold dark matter, caustic rings still form provided the fraction of axions is large enough. Ref. [14] places a lower limit of $\sim 35\%$ on the axion fraction based on the prominence of features in galactic rotation curves associated with caustic rings.

B. Caustic ring structure

Here we briefly describe the properties of an axially and reflection symmetric caustic ring and the flows associated with it [5]. The axial coordinate being irrelevant, the dark matter particles are conveniently labeled by two parameters (α, η) where η is the time when a given particle crosses the $z = 0$ plane and α the angle from the $z = 0$ plane at the time of the particle's most recent outer turnaround. The coordinates of the particles near the caustic

are given by

$$\begin{aligned}\rho &= a + \frac{1}{2}u(\eta - \eta_0)^2 - \frac{1}{2}s\alpha^2 \\ z &= b\alpha\eta\end{aligned}\tag{2.2}$$

where a , u , η_0 , s and b are constants characterizing the caustic ring. Since actual caustic rings are only approximately axially symmetric, the five constants vary to some extent along the ring. The caustic occurs where the Jacobian $|D_2(\alpha, \eta)| \equiv |\det \frac{\partial(\rho, z)}{\partial(\alpha, \eta)}|$ is zero. In the ρ - z plane, it takes the shape of a tricusp, shown in Fig. 2. The tricusp is the cross-section of a caustic ring. Its sizes, p in the ρ -direction and q in the z -direction, are given by [5]

$$\begin{aligned}p &= \frac{1}{2}u\eta_0^2 \\ q &= \frac{\sqrt{27}}{4} \frac{1}{\sqrt{\zeta}} p,\end{aligned}\tag{2.3}$$

where

$$\zeta = \frac{su}{b^2} = \frac{27}{16} \frac{p^2}{q^2}.\tag{2.4}$$

If $\zeta = 1$, the tricusp is invariant under rotations by 120° in the ρ - z plane.

It is convenient to write Eqs. (2.2) in terms of the rescaled coordinates $X = \frac{\rho-a}{p}$, $Z = \frac{z}{p}$:

$$\begin{aligned}X &= (T - 1)^2 - A^2 \\ Z &= \frac{2}{\sqrt{\zeta}} AT\end{aligned}\tag{2.5}$$

where $A = \alpha\sqrt{\frac{s}{u\eta_0^2}}$ and $T = \frac{\eta}{\eta_0}$. For a given point (X, Z) near the caustic, the parameters (T, A) of particles at that point are found by solving the quartic equation:

$$X = (T - 1)^2 - \frac{\zeta Z^2}{4T^2},\tag{2.6}$$

and setting $A = \frac{\sqrt{\zeta}Z}{2T}$. Each real solution corresponds to a flow of dark matter particles through that point. There are two flows through each point outside the tricusp, and four flows through each point inside. The density of the flow corresponding to a real solution (A_j, T_j) , $j = 1, \dots, K$ with $K = 2$ or 4 , is

$$d_j(\rho, z) = \frac{1}{2pb\rho} \frac{dM}{d\Omega d\eta} \frac{\cos(\alpha_j)}{|(T_j - 1)T_j + A_j^2|}\tag{2.7}$$

where $\frac{dM}{d\Omega d\eta}$ is the infall rate, i.e. the mass of dark matter particles falling in per unit time per unit solid angle. The velocity vector of the j th flow has components

$$\begin{aligned}v_{j\rho} &= u\eta_0(1 - T_j) \\ v_{jz} &= -u\eta_0 \frac{Z}{2T_j} \\ v_{j\phi} &= \sqrt{v^2 - v_{j\rho}^2 - v_{jz}^2}\end{aligned}\tag{2.8}$$

where v is the speed of the flow, and the ϕ -direction is $\hat{\phi} = \hat{\rho} \times \hat{z}$. For an axially symmetric caustic ring whose center coincides with the Galactic Center, $\hat{\rho}$ points radially outward, \hat{z} points toward the Galactic North Pole and $\hat{\phi}$ in the direction of Galactic rotation.

C. Model properties

The Caustic Ring Model is described in detail in ref. [4]. Here we only list the properties directly relevant to our discussion of the Gaia triangles and the M31 rotation curve. The model assumes that the flow of dark matter particles in a galactic halo is self-similar in time [25, 26], and axially symmetric. It gives the overall phase-space distribution of a disk galaxy’s halo in terms of the galaxy’s rotation velocity v_{rot} and a parameter j_{max} which is a dimensionless measure of the galaxy’s angular momentum. The model predicts a disk galaxy to have caustic rings in the galactic plane at radii given approximately by [27]:

$$a_n \simeq \frac{40 \text{ kpc}}{n} \left(\frac{v_{\text{rot}}}{220 \text{ km/s}} \right) \left(\frac{j_{\text{max}}}{0.18} \right) , \quad (2.9)$$

where $n = 1, 2, 3, \dots$. More precise predictions for the caustic ring radii are given in ref. [4]. The n th caustic ring forms in the flows of particles experiencing the n th inner turnaround in their history. The nominal values $v_{\text{rot}} \simeq 220 \text{ km/s}$ and $j_{\text{max}} \simeq 0.18$ apply to our Milky Way galaxy. The length scale in the $a_n \approx \frac{40\text{kpc}}{n}$ prediction for the Milky Way is set by the assumption that the radius of the solar orbit is 8.5 kpc. Four rings are therefore predicted to lie outside the solar orbit and the fifth just inside. The model is not so detailed as to predict the sizes p and q of the caustic ring cross-sections. Values of p/a estimated from rises in the Milky Way rotation curve range from 0.016 to 0.1 [20].

When the Caustic Ring Model was proposed, the observational evidence claimed for caustic rings raised a puzzle because caustic rings require the velocity field to have net overall rotation whereas the velocity field of ordinary CDM is irrotational. As mentioned already, axion Bose-Einstein condensation resolves this puzzle because cold dark matter axions thermalize sufficiently fast by gravitational self-interactions that almost all go to the lowest energy available state consistent with the angular momentum acquired by tidal torquing and that state is one of rigid rotation on the turnaround sphere. It was shown in ref. [15] that axion Bose-Einstein condensation justifies the Caustic Ring Model in all its aspects, including the fact that the caustic rings lie in the galactic plane, the magnitude of the parameter j_{max} and the pattern, Eq. (2.9), of caustic ring radii.

Ref. [14] analyzed the behavior of the vortices that form in the axion BEC constituting galactic halos. Unlike the vortices in superfluid ^4He , the vortices in axion BEC are mutually attractive and combine into one Big Vortex along the rotation axis of a disk galaxy. This results in a modification of the Caustic Ring Model since the infall was assumed to be isotropic [4] in the original formulation. The presence of a Big Vortex causes a depletion along the rotation axis and a compensating enhancement along the equatorial plane. The enhancement along the equatorial plane serves to explain why the bumps in galactic rotation curves attributed to caustic rings are so prominent. It had been noted in ref. [20] that the rises in the Milky Way rotation curve attributed to caustic rings are approximately a factor 4 larger than expected. The presence of a Big Vortex resolves this puzzle because caustic rings are formed in the flows of particles falling in and out close to the Galactic Plane where the density is enhanced. When estimating the densities of the flows associated with the nearby 5th caustic ring in Section IV, we will assume that there is a Big Vortex and that the densities are enhanced by a factor 4 compared to the predictions of ref. [4].

D. Summary of previous evidence

Several observations have been previously claimed as supporting evidence for the Caustic Ring Model. We briefly review these observations here.

1. Combined rotation curve

Caustic rings produce bumps at their locations in the rotation curves of galaxies [5, 27]. The extended and well measured rotation curves of 32 galaxies, published in refs. [28], were analyzed in ref. [29]. The radial coordinate r in each rotation curve was rescaled according to

$$r \rightarrow \tilde{r} = r \left(\frac{220 \text{ km/s}}{v_{\text{rot}}} \right), \quad (2.10)$$

to remove the dependence of the caustic ring radii on v_{rot} ; see Eq. (2.9). The rescaled rotation curves were then added to each other. The combined rotation curve, shown in Fig. 3, has two peaks, one near 40 kpc and one near 20 kpc, with significance of 3.0σ and 2.6σ respectively. The presence and locations of the two peaks are explained if they are caused by the $n = 1$ and $n = 2$ caustic rings of dark matter in those galaxies.

2. Milky Way rotation curve [20]

The inner ($r < r_{\odot}$) Milky Way rotation curve derived [30] from the Massachusetts-Stony Brook North Galactic Plane CO Survey [31] shows a series of sharp rises between 3 and 8.5 kpc. Each rise starts with an upward kink and ends with a downward kink as expected for rises caused by caustic rings of dark matter [5]. The Caustic Ring Model predicts ten rises between 3 and 8.5 kpc, assuming the value of $j_{\text{max}} = 0.18$ derived earlier from the ratio of baryonic to dark matter contributions to the Milky Way rotation curve at the solar radius [26][4]. Allowing for ambiguities in identifying rises, the number of rises in the rotation curve between 3 and 8.5 kpc is in fact ten plus or minus one. When the predicted caustic ring radii are fitted to the radii where the rises start in the rotation curve, with j_{max} the only adjustable parameter, the remaining root mean square relative discrepancy is 3.1% [20].

The outer rotation curve ($r > r_{\odot}$) is less well measured, but it does have a prominent rise between 12.7 and 13.7 kpc [32, 33], which is the predicted location of the third caustic ring. Furthermore a ring of stars, named the “Monoceros Ring”, was discovered in the Galactic Plane at $r \sim 20$ kpc [34]. It is shown in refs. [35][23] that this ring of stars is a plausible outcome of the second caustic ring’s gravitational field.

3. IRAS triangle [20]

Looking in the direction tangent to a caustic ring, one may expect to observe the imprint of the ring’s tricusp cross section on ordinary matter. A triangular feature seen in the IRAS map in the direction of Galactic Coordinates $(l, b) = (80^{\circ}, 0^{\circ})$ has been interpreted as the imprint of the 5th caustic ring. Relevant parts of the IRAS map can be found at <https://www.phys.ufl.edu/~sikivie/triangle/>. The orientation of the IRAS triangle with respect to the Galactic Center and the Galactic Plane is consistent with the Caustic

Ring Model. Also, the position of the triangle on the sky matches the position of the sharp rise (between 8.28 and 8.43 kpc) in the Milky Way rotation curve attributed to the 5th caustic ring. However, no triangular feature along the other tangent direction to the 5th caustic ring was found in the IRAS map.

E. M31 rotation curve

Our nearest major Galactic Neighbor M31 is viewed almost edge-on from our location. Fig. 4 shows the rotation curve of M31 derived by Chemin et al. [36] from their HI survey of that galaxy. There are several bumps in this rotation curve on both the receding and approaching sides. The first or outermost bumps are approximately at 30 kpc, the second ones at 15 kpc, and the third at 10 kpc. These numbers are consistent with the relation $a_n \sim \frac{1}{n}$ predicted by the Caustic Ring Model. The first bumps near 30 kpc are well outside the last observed spiral arm (at $r \sim 25$ kpc) and they match perfectly on both sides. This strongly indicates the presence of a ring-like structure in the dark halo. We also note that, although the first bumps match perfectly, the second ones appear at slightly different radii on one side than the other. And the third bump from the receding side is missing. These discrepancies give an indication of how closely we may expect the idealizations of the model to be matched by reality. The fact that the third caustic ring does not show on the receding side may mean that it lies somewhat outside of the galactic plane there. It is worth mentioning that there are several sources for the rotation curve of M31 at smaller radii, summarized and compared in Ref. [37], and they do not all agree with each other.

F. Gaia triangles

We mentioned that the triangular feature seen in the IRAS map in the direction $(l, b) = (80^\circ, 0^\circ)$ is not matched by a similar feature on the other side, i.e. at $(-80^\circ, 0^\circ)$. However, the sky map recently released by the Gaia Collaboration [21, 22] has a triangular feature at $(l, b) = (-91^\circ, 0^\circ)$ as well as a feature at $(80^\circ, 0^\circ)$ matching the triangular feature in the IRAS map. See: <https://www.phys.ufl.edu/~sikivie/Gaiamap/>. We refer to the features as right and left triangles respectively. Relevant parts of the Gaia skymap are reproduced in Figs. 5 and 6. The shape and the orientation of the right triangle are consistent with the expected shape and orientation of a caustic ring imprint. The right triangle is farther from the Galactic Center and approximately 40% smaller than the triangle on the left, but we believe both are imprints of the 5th caustic ring. We attribute the asymmetry in location to a displacement, by 5.8° to the right, of the center of the caustic ring relative to the Galactic Center; see Fig. 7 for an illustration. The possibility that the ring is not a perfect circle between the two tangent points is discussed in Section IV.B.

The triangular features in the Gaia map are darker than their surroundings. Obscuration is generally due to dust. The obscuration is more uniform over the Gaia right triangle than over the Gaia left triangle. Assuming the background of star light to be uniform, we estimate the optical depth for light absorption τ_d is of order 1.7 over the area of the right triangle, and varying approximately from 0.9 to 3.0 over the area of the left triangle. The 3D dust map constructed in ref. [38] on the basis on Gaia, PANSTAR-1 and 2MASS data, also shows a feature in the direction of the left triangle; see Fig. 8. Unfortunately, the direction of the right triangle is not covered by this map. For a better understanding of the distribution

of dust in the direction of the left triangle, Fig. 9 shows the accumulated reddening in successive distance segments. Panels (b) and (c) of this figure have the most accumulated dust in the direction of interest. It seems that most of the dust making up the feature in Fig. 8 is situated between 0.8 kpc and 1.6 kpc. This is consistent with the location of the caustic ring in the left tangent direction based on the calculations in Section IV.

We performed an analysis of the statistical significance of the left and right triangular features in the Gaia skymap. The analysis is described in Appendix A.

When the IRAS triangle was first discussed as a candidate imprint of the 5th caustic ring [20], it was proposed that this feature is produced by gas and dust in thermal equilibrium in the gravitational field of the 5th caustic ring. However in ref. [23] it is shown that the features produced in this way are not as sharp as the observed features. Here we propose instead that the features are produced by dust that is entrained by the axion flows forming the caustic ring. The entrained dust particles have the same trajectories as the axions and thus make the same caustics. This would explain why the triangular features are sharp. Section III discusses the entrainment of dust particles by cold axion flows.

We also propose here an explanation why the right triangle does not show in the IRAS map whereas the left triangle does show. The caustic ring in the left tangent direction lies in the midst of the stellar activity associated with the Orion Spur of the Sagittarius Spiral Arm. The dust is heated there by stars and reradiates the heat in the infrared, where IRAS is sensitive. The caustic ring in the right tangent direction lies in a relatively quiet place. Its dust does not get heated sufficiently to show up in the IRAS map.

III. DUST ENTRAINMENT

In this section we discuss physical processes that may be responsible for the formation of the triangles observed in the IRAS and Gaia maps of the Milky Way. As mentioned in the previous section, we interpret the triangles as due to the entrainment of dust by the axion flows forming the nearby caustic ring. The dust particles follow the same trajectories as the axions and hence form the same caustics. We propose this as an explanation for the sharpness of the triangles. For the explanation to be plausible, it must be shown not only that dust is entrained by cold axion flows but also that the entrainment occurs in spite of the drag on the dust due to gas in the Galactic Disk. We first derive a formula for the friction on a dust particle moving with respect to a highly degenerate Bose-Einstein condensed axion fluid. The frictional force is inversely proportional to the temperature T of the axions. We next discuss the temperature that axion dark matter has today, and compare the friction of the axion fluid with the drag due to gas. Finally we consider dust-dust collisions and find that they plausibly explain why the features seen in the IRAS and Gaia maps are triangular rather than tricuspy.

A. Friction on a cold axion fluid

Cold dark matter axions thermalize by gravitational self-interactions in a regime, called the “condensed regime”, where their energy dispersion is much less than their thermalization rate. Their thermalization rate is of order [11, 12]

$$\Gamma \sim 4\pi Gnm^2\ell^2 \quad (3.1)$$

where G is Newton's gravitational constant, m is the axion mass, n is the number density of axions, and $\ell = \frac{1}{\delta p}$ their correlation length. δp is the momentum dispersion of the axion fluid. By definition, $\Gamma = 1/\tau$ where τ is the time scale over which each axion may change its momentum by order δp .

1. Scale of inhomogeneity vs. correlation length

The correlation length ℓ is unrelated to the scale of homogeneity and should not be confused with it [19]. To make precise this distinction consider a generic state of the cold axion dark matter fluid. Almost all axions are in a small number of particle states with almost identical wavefunctions. Let $\Psi_0(\vec{x}, t)$ be the wavefunction of one of those highly occupied states. It defines a flow of density $n(\vec{x}, t) = N_0 |\Psi_0(\vec{x}, t)|^2$, where N_0 is the number of particles in the state, and velocity field $\vec{v}(\vec{x}, t) = \frac{1}{m} \vec{\nabla} \text{Im} \ln \Psi_0(\vec{x}, t)$. Starting with an arbitrary Ψ_0 , one may construct a complete orthonormal set of wavefunctions [19]

$$\Psi_{\vec{k}}(\vec{x}, t) = \Psi_0(\vec{x}, t) e^{i\vec{k} \cdot \vec{\chi}(\vec{x}, t)} \quad (3.2)$$

where the $\vec{\chi}(\vec{x}, t)$ are the co-moving coordinates implied by the velocity field $\vec{v}(\vec{x}, t)$ and the requirement that the particle density is constant in co-moving coordinate space. For small \vec{k} the particle states $\Psi_{\vec{k}}$ are very close to Ψ_0 , having the same density field and almost the same velocity field. We may write the axion field in the non-relativistic limit as

$$\phi(\vec{x}, t) = \sum_{\vec{k}} \frac{1}{\sqrt{2m}} [e^{-imt} \Psi_{\vec{k}}(\vec{x}, t) a_{\vec{k}}(t) + e^{imt} \Psi_{\vec{k}}^*(\vec{x}, t) a_{\vec{k}}^\dagger(t)] \quad (3.3)$$

where $a_{\vec{k}}(t)$ and $a_{\vec{k}}^\dagger(t)$ are annihilation and creation operators satisfying canonical equal-time commutation relations. Let $N_{\vec{k}} = \langle \Phi | a_{\vec{k}}^\dagger a_{\vec{k}} | \Phi \rangle$ be the particle state occupation numbers in a state $|\Phi\rangle$ of the axion fluid. The correlation length in comoving coordinates is $\ell = \frac{1}{\delta k}$ where

$$\delta k = \sqrt{\frac{1}{N} \sum_{\vec{k}} \vec{k} \cdot \vec{k} N_{\vec{k}}} \quad (3.4)$$

and $N = \sum_{\vec{k}} N_{\vec{k}}$ is the total number of particles. If a Bose-Einstein condensate (BEC) forms, a fraction of order one of the total number N of particles go to the same particle state, e.g. the state of wavefunction Ψ_0 . In that case the two-point axion field equal-time correlation function is [19]

$$\langle \Phi | \phi(\vec{x}, t) \phi(\vec{y}, t) | \Phi \rangle = \frac{N_0}{2m} (\Psi_0^*(\vec{x}, t) \Psi_0(\vec{y}, t) + c.c.) + \dots \quad (3.5)$$

where $N_0 \sim N$ is the number of particles in the condensate, and the dots represent the contributions, which fall off exponentially or as a power law, of particles that are not in the condensate. Eq. (3.5) shows that a BEC is 'perfectly' correlated over its full extent, i.e. its correlation length ℓ is the size of the region over which $\Psi_0(\vec{x}, t)$ has support. In contrast, the scale of inhomogeneity s of the condensate is the distance scale over which the density $n(\vec{r}, t)$ varies by order one. ℓ can be arbitrarily large compared to s . In the axion case, s may be the size of mini-clusters or of galaxies whereas ℓ may be the size of the horizon.

2. Thermal relaxation

In estimating the frictional force of the axion fluid on a dust particle, we will assume that the axion fluid has thermalized completely. However, it is not clear to us to what extent the axion fluid has thermalized. The assumption of complete thermalization is made to allow us to make an estimate of the aforementioned drag. If fully thermalized the axion fluid consists of a BEC of N_0 axions in a single state, of wavefunction Ψ_0 , plus a thermal distribution of axions with chemical potential $\mu = m$ and temperature T . The wavefunction Ψ_0 is time-dependent on the Hubble time scale since this is the time scale over which large scale structure grows by gravitational instability. The thermal relaxation time scale is much shorter than that as we now show in the case, used as an example, of the cold axion flow forming the nearby caustic ring. The flow extends over a region of order 100 kpc in size. Its correlation length is that size, $\ell \sim 100$ kpc, regardless of the inhomogeneities in it. Its average energy density $nm \sim 10^{-26}$ gr/cc over that length scale [4]. Eq. (3.1) implies that its relaxation rate is

$$\Gamma \sim \frac{10^4}{\text{sec}} \left(\frac{m}{10^{-5} \text{ eV}} \right) \quad . \quad (3.6)$$

The relaxation rate exceeds the Hubble rate by some 21 orders of magnitude.

The relaxation process can be described heuristically as follows. The axion fluid consists of a huge number of axions occupying a small number of states with the wavefunctions given in Eq. (3.2). The average gravitational field produced by the axion fluid is $g(\vec{x}, t)$ sourced by the density $mn(\vec{x}, t) = mN_0|\Psi_0(\vec{x}, t)|^2$. However, the actual gravitational field fluctuates around this average because the actual density is modulated over a distance scale $\ell = 1/\delta k$. The root mean square deviation of the gravitational field from its average value $g(\vec{x}, t)$ is

$$\sigma_g \sim 4\pi G n m \ell \quad . \quad (3.7)$$

As discussed in ref. [12], σ_g is the outcome of a random walk, the sum of many terms with random phases. The average gravitational field $g(\vec{x}, t)$ determines the dynamical evolution of the axion fluid. Since we are interested in the relaxation of the axion fluid, as opposed to its overall dynamical evolution, we ignore $g(\vec{x}, t)$ henceforth. We set it equal to zero by adopting a reference frame in which the fluid is freely falling.

The gravitational field fluctuations change all the particle momenta by amounts of order δp in a time $\tau \sim \frac{\delta p}{m\sigma_g}$. Substituting Eq. (3.7) yields Eq. (3.1) as an estimate of the relaxation rate. Relaxation results in momentum distributions of ever increasing likelihood. Although far from thermal equilibrium to start with, the axion fluid may reach near-thermal equilibrium by gravitational self-interactions before the present. It may also absorb heat from other species, e.g. from baryons [12]. There is however a maximum temperature the axion fluid may become fully thermalized at by gravitational self-interactions. Since the axions may change their momenta by order δp in a time of order τ , they can at most reach velocities of order

$$v_m \sim \sigma_g t_0 \sim 4\pi G n m t_0 \ell \sim 0.4 \left(\frac{\Omega_a}{0.27} \right) \left(\frac{\ell}{t_0} \right) \quad . \quad (3.8)$$

Here we have set $nm = \Omega_a \rho_{\text{crit}}(t_0)$, where $\rho_{\text{crit}}(t_0)$ is the present critical energy density for closing the universe and Ω_a is the fraction thereof in axions. This implies a maximum temperature

$$T_m \sim \frac{1}{3} m v_m^2 \sim 6 \cdot 10^{-2} m \left(\frac{\ell}{t_0} \right)^2 \left(\frac{\Omega_a}{0.27} \right)^2 \quad (3.9)$$

that axions may become fully thermalized at before today.

3. Frictional force

Since the gravitational field produced by the axion fluid at any space-time point is a sum of many terms with random phases, with σ_g the average outcome, the probability that the gravitational field has value between g and $g + dg$ is

$$\mathcal{P}(g)dg = \frac{1}{\sqrt{2\pi}\sigma_g} e^{-\frac{1}{2}\left(\frac{g}{\sigma_g}\right)^2} dg \quad (3.10)$$

by the central limit theorem. Eq. (3.10) holds in the absence of the dust particle, whose presence we have ignored so far. In the presence of the dust particle, the random walk becomes biased toward gravitational fields that slow down the dust particle with respect to the axion fluid because such slowdown is accompanied by an increase in the energy, and therefore the entropy, of the axion fluid. Let M be the mass of the dust particle and $\vec{v} = v\hat{n}$ its velocity with respect to the axion fluid. A gravitational field of strength $-g\hat{n}$ for the duration τ slows down the dust particle by $\Delta v = -g\tau$ and therefore increases the energy of the axion fluid by $\Delta E = Mv|\Delta v| = Mg\tau v$. Its entropy increases by $\Delta S = \frac{1}{T}\Delta E$. As Boltzmann pointed out, a ΔS increase in entropy signifies an increase by the factor $e^{\Delta S}$ in the number of available microstates and therefore an increase by that factor in the relative probability to have the gravitational field that causes it. Thus in the presence of the dust particle, the probability distribution of the gravitational field at the dust particle's location is modified from Eq. (3.10) to

$$\mathcal{P}'(g)dg = Ce^{-\frac{1}{2}\left(\frac{g}{\sigma_g}\right)^2 + \Delta S} dg \quad (3.11)$$

where

$$\Delta S = \frac{1}{T}Mg\tau v = \frac{Mv}{mT\ell} \frac{g}{\sigma_g} \quad (3.12)$$

and C is a normalization constant determined by the requirement that the total probability is one. The deceleration d of the dust particle is the average of the g -distribution in Eq. (3.11). One readily finds

$$d = \frac{Mv}{mT\ell}\sigma_g \sim 4\pi GnMv \frac{1}{T} \quad (3.13)$$

This formula for friction is different, and applies in different circumstances, from the standard formula for dynamical friction [41, 42]. Both formulae, Eq. (3.13) and the standard formula whose RHS is $4\pi G^2 nmMv^{-2} \ln(\Lambda)$ where Λ is the ratio of maximum to minimum impact parameters, describe the drag on a heavy mass M moving through a fluid, as a result of the gravitational interactions of the heavy mass with the particles in the fluid. The standard formula assumes that the particles in the fluid do not interact among themselves. Only their gravitational interaction with the heavy mass is taken into account. They get scattered by the heavy mass plowing through and as a result remove kinetic energy from it, slowing it down. Eq. (3.13) assumes instead that the particles in the fluid interact with one another sufficiently strongly that they thermalize while interacting gravitationally with the mass M .

Eq. (3.13) is not expected to be valid when M is large, such as the mass of a star or even a small planet, because the Gaussian distribution in Eq. (3.11) does not extend to arbitrarily

large values of g . For example, for $M = 10^{25}$ gr, $m = 10^{-5}$ eV, $T = 10^{-9}$ eV, and $\ell = 100$ kpc, Eq. (3.13) would need the Gaussian to extend to $g \sim 10^{44} v \sigma_g$, which it cannot possibly reach by the aforementioned random walk.

B. Axion temperature

The correlation length ℓ of the cold axion fluid, just after it was produced by vacuum realignment during the QCD phase transition, is of order the horizon at that time. Subsequently ℓ is stretched by the expansion of the universe. The relaxation rate Γ , decreasing as $a(t)^{-1}$ where $a(t)$ is the scale factor, exceeds the Hubble expansion rate $H(t) = \frac{1}{2t}$ when the photon temperature is of order 1 keV [11, 12]. The cold axions form a BEC then and ℓ grows to be of order the horizon at that time. Whereas Bose-Einstein condensation occurs on the τ time scale, full thermalization takes much longer [12, 43]. Nonetheless, as was indicated above, nearly full thermalization may occur before the present and temperatures as high as $6 \cdot 10^{-2} m$ may possibly be reached. The final temperature depends on the amount of heat that the axion fluid absorbs and thermalizes.

1. Heat from axions

The first and most obvious source of heat is the kinetic energy the cold axions themselves have because the axion field is inhomogeneous on the horizon scale at the QCD phase transition. We assume here that the axion field was not homogenized by inflation, so that the kinetic energy of cold axions is the highest possible. We will see that even then the heat associated with the initial kinetic energy of cold axions is negligible compared to the heat the axion fluid absorbs by cooling baryons (see below.). The axion kinetic energy density is

$$\rho_{a,\text{kin}}(t) = \frac{(\delta p(t))^2}{2m} n(t) \sim \Omega_a \rho_{\text{crit}}(t_0) \frac{1}{2t_1^2 m^2} \frac{a(t_1)^2}{a(t)^5} \quad (3.14)$$

where $a(t)$ is the cosmological scale factor normalized such that $a(t_0) = 1$, and [10]

$$t_1 \simeq 1.7 \cdot 10^{-7} \text{ sec} \left(\frac{10^{-5} \text{ eV}}{m} \right)^{\frac{1}{3}} \quad (3.15)$$

is the time at which the axion mass effectively turns on during the QCD phase transition. The last statement in Eq. (3.14) follows from $\delta p(t) \sim \frac{1}{t_1} \frac{a(t_1)}{a(t)}$ as is the case if inflation does not homogenize the axion field. Let us call t_* the time when cold axions fully thermalize among themselves. They have at that time temperature T_* :

$$\rho_{a,\text{kin}}(t_*) = 0.128 (m T_*)^{\frac{3}{2}} T_* \quad (3.16)$$

provided $T_* \ll m$, as will be the case. Combining Eqs. (3.14) and (3.16) yields

$$T = T_* a(t_*)^2 \sim 10^{-14} \text{ eV} \Omega_a^{\frac{2}{5}} \left(\frac{10^{-5} \text{ eV}}{m} \right)^{\frac{19}{15}} \quad (3.17)$$

for the axion temperature today. Note that T does not depend on t_* because the axions are non-relativistic both before and after they thermalize.

2. Heat from baryons

The cold axion fluid may absorb heat from other species. Ref. [44] considered the possibility that the axions cool the photons and offered this as an explanation for the Li anomaly in primordial nucleosynthesis. However, photon cooling can only occur marginally because it requires the correlation length to be as large as the horizon whereas by causality the correlation length must be at least somewhat shorter. The observations of the cosmic microwave background anisotropies by the Planck Collaboration indicate an effective number of neutrinos [45] consistent with the absence of photon cooling. So we ignore heat from photon cooling. On the other hand, cooling of baryons by axion BEC occurs robustly according to the arguments of ref. [12]. The reported observation by the EDGES Collaboration [46] of the trough in the cosmic microwave radiation spectrum due to its absorption by neutral hydrogen at cosmic dawn indicates that baryons are significantly colder at that time than expected under standard assumptions. The EDGES observation may be viewed as confirmation that axion BEC did indeed cool baryons [47, 48].

If axions and baryons reach full kinetic equilibrium before today, a lower limit on the heat transfer from baryons to axions is the kinetic energy that baryons would have today in the absence of axion cooling. Keeping in mind that baryons and photons decouple from each other at a redshift $z_{\text{dec}} \sim 160$, the baryon kinetic energy density today, in the absence of axion cooling, is

$$\rho_{b,\text{kin}}(t_0) \simeq \frac{3}{2} T_\gamma(t_0) \Omega_b \rho_{\text{crit}}(t_0) \frac{1}{m_b} \frac{1}{1 + z_{\text{dec}}} \quad , \quad (3.18)$$

where $T_\gamma(t_0) \simeq 2.7$ K is the present photon temperature, $\Omega_b \simeq 0.05$ is the present energy density fraction in baryons, and $m_b \simeq \text{GeV}$ is an average baryon mass. Using Eq. (3.16), baryon cooling by axions implies

$$T > 0.7 \cdot 10^{-7} \text{ eV} \left(\frac{10^{-5} \text{ eV}}{m} \right)^{\frac{3}{5}} \quad , \quad (3.19)$$

if axions and baryons reach full kinetic equilibrium. The RHS of Eq. (3.19) exceeds, or saturates depending on the axion mass, our earlier estimate Eq. (3.9) of the highest temperature that the axion fluid may become fully thermalized at.

C. Dust entrainment

As mentioned in Section II, dark matter axions rethermalize sufficiently fast by gravitational self-interactions while they fall in and out of a galactic gravitational potential well that they almost all go to the lowest energy state consistent with the angular momentum they have acquired by tidal torquing interactions with neighboring galaxies. That state is one of rigid rotation on the turnaround sphere. As a result dark matter axions fall in with a rotational velocity field and make caustic rings.

We will assume here, for simplicity, that the dark matter is entirely axions, or axion-like particles (as opposed to a mixture of axions and ordinary CDM). The infalling axions entrain gas and dust, but not stars for the reason stated at the end of subsection III.A.3. The gas is not collisionless, of course. Gas falling in with the axions collides with gas already in the galaxy and soon leaves the phase-space sheet on which the axions lie. Whereas the angular momentum of the gas is approximately conserved, the kinetic energy associated with its

radial motion is dissipated into radiation. As a result the gas settles in a rotating disk, where it participates in star formation. The stars formed rotate along with the gas. Dust is produced in the late stages of stellar evolution.

We consider dust particles of typical size $D \sim 5 \cdot 10^{-5}$ cm [49], and mass $M \sim 3 \cdot 10^{-13}$ gr. Eq. (3.13) implies that the speed of a dust particle relative to the axion flow decreases according to $v(t) = v(0)e^{-\gamma t}$ with

$$\gamma \sim 4\pi G\rho \frac{M}{m} \frac{1}{T} \sim \frac{4 \cdot 10^4}{t_0} \left(\frac{\rho}{10^{-26} \text{ gr/cc}} \right) \left(\frac{10^{-5} \text{ eV}}{m} \right) \left(\frac{M}{3 \cdot 10^{-13} \text{ gr}} \right) \left(\frac{10^{-9} \text{ eV}}{T} \right) \quad , \quad (3.20)$$

implying that the dust particle is entrained in the absence of any other forces acting on it, even if the axion temperature is as high as we believe it can be. We now consider the effect of dust-gas and dust-dust collisions.

1. Dust-gas collisions

The density of gas in the solar neighborhood is approximately $\rho_g \sim 3 \cdot 10^{-24}$ gr/cc, comprising of order one atom or molecule per cm^3 [42]. The cross-section for hard-scattering on a dust particle is of order $\sigma \sim D^2 \sim 2.5 \cdot 10^{-9}$ cm^2 . A dust particle moving with velocity v_g relative to the gas experiences a deceleration

$$d_g \sim \frac{\rho_g \sigma (v_g)^2}{M} = 2.2 \cdot 10^{-5} \frac{\text{cm}}{\text{sec}^2} \left(\frac{\rho_g}{3 \cdot 10^{-24} \text{ gr/cc}} \right) \cdot \left(\frac{\sigma}{2.5 \cdot 10^{-9} \text{ cm}^2} \right) \left(\frac{3 \cdot 10^{-13} \text{ gr}}{M} \right) \left(\frac{v_g}{300 \text{ km/s}} \right)^2 \quad . \quad (3.21)$$

At the caustic the axions flow relative to the gas with velocity 300 km/s in the direction of Galactic Rotation. The speed of the dust particle with respect to the axion flow is $v = 300 \text{ km/s} - v_g$. The acceleration of the dust particle in the direction of Galactic Rotation due to its friction on the axion flow is

$$d \sim 2.7 \cdot 10^{-6} \frac{\text{cm}}{\text{sec}^2} \left(\frac{\rho}{10^{-26} \text{ gr/cc}} \right) \left(\frac{10^{-5} \text{ eV}}{m} \right) \left(\frac{M}{3 \cdot 10^{-13} \text{ gr}} \right) \left(\frac{10^{-9} \text{ eV}}{T} \right) \left(\frac{v}{300 \text{ km/s}} \right) \quad (3.22)$$

according to Eq. (3.13). Setting $d_g = d$ yields a second order polynomial equation for v_g whose relevant solution is

$$v_g = [\sqrt{\xi^2 + 2\xi} - \xi] 300 \text{ km/s} \quad (3.23)$$

with

$$\xi \sim 6 \cdot 10^{-2} \left(\frac{\rho}{10^{-26} \text{ gr/cc}} \right) \left(\frac{10^{-5} \text{ eV}}{m} \right) \left(\frac{M}{3 \cdot 10^{-13} \text{ gr}} \right)^2 \cdot \left(\frac{10^{-9} \text{ eV}}{T} \right) \left(\frac{2.5 \cdot 10^{-9} \text{ cm}^2}{\sigma} \right) \left(\frac{3 \cdot 10^{-24} \text{ gr/cc}}{\rho_g} \right) \quad . \quad (3.24)$$

Several factors on the RHS of Eq. (3.24) are poorly known, including the axion mass and the temperature of the axion fluid. We consider two specific cases for illustrative purposes. If $m \sim 10^{-5}$ eV and the axion fluid is not heated by the baryons, or anything else, so that

$T \sim 10^{-14}$ eV, $\xi \sim 6 \cdot 10^3$ and therefore $v \sim 26$ m/s. The dust particle follows the axion fluid very closely in this case. If on the other hand $m \sim 10^{-6}$ eV and $T \sim 6 \cdot 10^{-8}$ eV, the latter being our estimate Eq. (3.9) of the highest temperature the axions may become thermalized at when $m \sim 10^{-6}$ eV, then $\xi \sim 0.01$ and $v_g \sim 39$ km/s. The dust particles move more slowly than the axion fluid in this case; their velocity is 259 km/s in the Galactic Rest Frame vs. 520 km/s for the axion fluid. However, even though they move more slowly, we may still expect the dust particles to follow the same trajectories as the axion fluid and hence form the same caustics.

Collisions with gas diffuses the dust flow by imparting random transverse velocities to the dust particles, but not so much as to prevent caustic formation. Indeed, the number of dust-gas collisions during one pass of a dust particle through the Galactic Disk is order 10^{14} , each collision producing a random transverse velocity of order $v_g m_g / M$, which is less than $3 \cdot 10^{-10}$ km/s. So the rms transverse velocity acquired is less than 3 m/s.

2. Dust-dust collisions

The density n_d of the dust flows forming the triangular features in the Gaia map may be estimated from the optical depth $\tau_d \sim 2$ for the absorption of light over the area of the triangles. The absorption length $\lambda \sim \frac{1}{n_d \sigma} \sim L / \tau_d$ where $L \sim 1$ kpc is the depth over which light travels through the tricusp volume of the caustic ring in the tangent directions and $\sigma \sim D^2 \sim 2.5 \cdot 10^{-9}$ cm² is the absorption cross-section. This implies $n_d \sim 270 / (\text{km})^3$. We take the cross-section for hard scattering of a dust particle on a dust particle to be of order $\sigma_d \sim 3 D^2 \sim 0.75 \cdot 10^{-8}$ cm². Hence the mean free path between dust-dust scatterings $\lambda_d \sim \frac{1}{\sigma_d n_d} \sim 160$ pc whereas the distance traveled transversely within the tricusp, where each flow is one of four different flows, is of order 100 pc, implying an optical depth for hard scattering of order 0.6. That the optical depth is of order one provides a plausible explanation why the caustic imprints seen in the IRAS and Gaia maps are triangular rather than tricusp. Indeed, the trajectories forming the cusps encounter very high dust densities there.

All trajectories through the tricusp pass through caustic folds, some trajectories participate in the formation of caustic folds, and among those some also participate in the formation of caustic cusps. The fact of going through or participating in the formation of a fold does not increase the optical depth for scattering with other dust much because the density at a fold increases as $n \propto \frac{1}{\sqrt{h}}$ where h is the distance to the fold surface and the $\frac{1}{\sqrt{h}}$ singularity is integrable. On the other hand, the density diverges as $\frac{1}{h}$ when a cusp is approached in the plane of the cusp [5], leading to a logarithmic divergence in the optical depth for the flows forming the cusp. Moreover, three flows participate in the formation of a cusp whereas only two flows participate in the formation of a fold. Since the optical depth is order one, it is plausible that dust-dust collisions mess up the formation of cusps without messing up the formation of folds. The sides of a triangular feature associated with a caustic ring seen in a tangent direction indicate then the location of folds whereas the cusps are effectively erased. A prediction of this interpretation is that the appearance of a tricusp imprint becomes more cuspy when the optical depth for obscuration by the dust in the feature is less, i.e. fainter caustic ring imprints will look more tricusp.

IV. BIG FLOW PROPERTIES

We use the Gaia triangles to determine the properties of the four prominent flows on Earth associated with the nearby caustic. Knowledge of their densities and velocities helps axion dark matter searches, particularly those using the cavity method [50] and the echo method [51]. We call the four flows Big, Little, Up and Down. We estimate the Sun's position relative to the nearby caustic ring by interpolating between the triangular features observed in the left and right tangent directions to the ring. Then, from the Sun's position relative to the nearby caustic, we derive the flow velocities with respect to the Local Standard of Rest (LSR). We also estimate the flow densities, and our errors on the various flow properties.

From the triangles, we find that the caustic ring center is displaced from the Galactic Center by 5.8° to the right. However, our distance from the caustic ring center $r_{\odot C}$ is not known. If our distance to the inner tangent point is between 0.8 and 1.2 kpc (based on panel b of Fig. 9), then $r_{\odot C}$ has a value between 7.2 and 10.8 kpc. We assume $r_{\odot C} = 8.5$ kpc in our estimates below. We also assume the velocity of the LSR to be $v_{\text{rot}} = 220$ km/s in the direction of Galactic Rotation. All our distances scale as $r_{\odot C}$, and all our velocities as v_{rot} . For this reason, we do not quote any errors associated with imperfect knowledge of $r_{\odot C}$ and v_{rot} . If $r_{\odot C}$ is found to differ from 8.5 kpc, one should simply multiply all our distances ($a, p, q \dots$) by $r_{\odot C}/8.5$ kpc. Likewise for v_{rot} . Our estimates of the flow velocities are independent of $r_{\odot C}$. Our estimates of the flow directions are independent of both $r_{\odot C}$ and v_{rot} since they are determined by ratios of velocity components and each component scales as v_{rot} . There is however an error in the flow directions associated with uncertainty of the ratio v/v_{rot} where v is the speed of the flows forming the 5th caustic ring. According to the model [4], $v = 520$ km/s when $v_{\text{rot}} = 220$ km/s. $v = 520$ km/s is the central value we use here. From the success of the model in describing the pattern of caustic ring radii in the Milky Way [20], we estimate that the error on v/v_{rot} is less than 3%.

A. Previous estimates

When only the left triangular feature in the IRAS sky map was known, the radius a and width p of the 5th caustic ring were estimated [20] as:

$$\begin{aligned} a &\simeq 8.31 \text{ kpc} \\ p &\simeq 130 \text{ pc} , \end{aligned} \tag{4.1}$$

by assuming the ring to be axially symmetric and centered at the Galactic Center. The Sun would then be outside the tricusp implying that there are two flows through our location, called Big and Little. Their densities and velocities were estimated to be [4]:

$$\begin{aligned} d_+ &\simeq 1.5 \times 10^{-24} \frac{\text{g}}{\text{cm}^3} \\ d_- &\simeq 0.15 \times 10^{-24} \frac{\text{g}}{\text{cm}^3} \\ \vec{v}_\pm &\simeq (\pm 120 \hat{\rho} + 505 \hat{\phi}) \frac{\text{km}}{\text{s}} \end{aligned} \tag{4.2}$$

where $\hat{\rho}$ points radially outward from the Galactic Center and $\hat{\phi}$ points in the direction of Galactic Rotation. Because of an ambiguity in the sign of η_0 , it is not clear which flow has

the larger density. If $\eta_0 < 0$, the flow of velocity \vec{v}_\pm has density d_\mp . If $\eta_0 > 0$, the flow of velocity \vec{v}_\pm has density d_\pm .

In Ref. [14] it was argued that formation of a Big Vortex in the axion dark matter fluid results in an enhanced dark matter density in the caustic rings. Any rotating BEC must have vortices. Whereas the vortices in superfluid ^4He are repulsive, those in axion BEC are attractive. Most of them merge to form a Big Vortex along the symmetry axis of the galaxy, enhancing the dark matter density in the Galactic Plane. We assume this enhancement to be approximately by a factor 4 because this accounts for the prominence of the bumps in the Milky Way rotation curve attributed to caustic rings [14, 20]. The density estimates in Eq. (4.2) assume isotropic infall [4]. Assuming the presence of a Big Vortex, they are modified to $d_+ \sim 6 \times 10^{-24}$ and $d_- \sim 0.6 \times 10^{-24}$ g/cc. Let us emphasize that densities near caustics have in any case large uncertainties because they are sensitive to position.

B. The Sun's position relative to the nearby caustic

The Galactic Coordinates (l, b) of the vertices of the left triangle as observed in both the IRAS and Gaia sky maps are: $(77.86^\circ \pm 0.04^\circ, 3.3^\circ \pm 0.5^\circ)$, $(83.1^\circ \pm 0.4^\circ, 0.25^\circ \pm 0.15^\circ)$, $(77.85^\circ \pm 0.04^\circ, -2.4^\circ \pm 0.2^\circ)$. Those of the right triangle observed in the Gaia sky map are: $(-89.35^\circ \pm 0.05^\circ, 1.25^\circ \pm 0.05^\circ)$, $(-92.95^\circ \pm 0.05^\circ, -0.65^\circ \pm 0.05^\circ)$, $(-89.55^\circ \pm 0.05^\circ, -2.27^\circ \pm 0.03^\circ)$. The right triangle is located farther from the Galactic Center compared to the left triangle. We interpret this to mean that the center of the 5th caustic ring is displaced from the Galactic Center to the right as shown in Fig. 7. Assuming that the inner side of the caustic ring is an exact circle between the left and right tangent points, its center is located in the direction of Galactic Longitude $l = -5.80^\circ \pm_{-0.04^\circ}^{+0.05^\circ}$. For the nominal value of our distance from the caustic ring center, $r_{\odot C} = 8.5$ kpc, and assuming the caustic ring to be circular, its radius is $a = (8.448 \pm_{-0.001}^{+0.001})$ kpc. Assuming that the caustic ring between the two tangent points lies in the plane determined by its center and the two midpoints of the inner edges of the triangles, we find that the caustic ring plane is tilted to the right by $\theta_t = 0.48^\circ \pm_{-0.20^\circ}^{+0.20^\circ}$ relative to the Galactic Plane. We discuss below the errors due to failure of the assumption that the caustic ring is exactly circular and planar between the two tangent points, and include them in the error budget of the flow velocity vectors.

The location of the Sun relative to the caustic is specified by the horizontal and vertical sizes of the tricusp near the Sun (p_\odot and q_\odot), the horizontal distance of the Sun ($x_\odot = r_{\odot C} - a$) from the inner side of the tricusp and its perpendicular distance (z_\odot) from the plane. We calculate the central values of these quantities based on the following assumptions: 1) the observed features are triangles inscribed by the tricusp; see Fig. 10, 2) the caustic ring is planar with its center displaced from the Galactic Center, 3) it has constant a , whereas p and q vary linearly between the left and right tangent directions. The resulting central values and errors are:

$$\begin{aligned}
 p_\odot &= (78.5 \pm_{-20.3}^{+23.7}) \text{ pc} , \\
 q_\odot &= (113.5 \pm_{-10.4}^{+10.5}) \text{ pc} , \\
 x_\odot &= (52.1 \pm_{-8.6}^{+0.7}) \text{ pc} , \\
 z_\odot &= (0.8 \pm_{-0.4}^{+0.5}) \text{ pc} .
 \end{aligned} \tag{4.3}$$

We now briefly discuss the various sources of uncertainty.

The largest source of uncertainty derives from ambiguity in estimating the horizontal size p of the tricusp. If the observed triangles represent the cross-sections of the caustic ring near the inner tangent points, the linearly interpolated value of p near the Sun is $p_{\odot} = (95.6^{+6.6}_{-6.5})$ pc where the uncertainties are associated with reading the vertices. On the other hand, if the outer vertices of the observed triangles tell us the directions of the outer tangent points, then $p_{\odot} = (61.4^{+1.9}_{-2.1})$ pc. We take the central value of p_{\odot} to be 78.5 pc. The error on p_{\odot} stated in Eq. (4.3) includes an additional contribution from the possible failure of the assumption of circularity of the ring, as discussed below. The uncertainty on q_{\odot} is much less than that on p_{\odot} because it is determined by the inner side of the triangles. The uncertainty in q_{\odot} is due to the errors associated with reading the vertices.

For a planar caustic ring, the value of z_{\odot} is $(0.8^{+0.5}_{-0.4})$ pc, including uncertainties from the vertices. We consider the case of a non-planar caustic ring where its outer cusp has height $z(\phi) = A \cos \phi$ from a plane where ϕ is the azimuthal angle about the caustic ring center and $\phi = 0$ is the azimuth of the Sun. The error in z_{\odot} associated with non-planarity is less than 0.3 pc if $A < 200$ pc. $A > 200$ pc seems unlikely since the caustic ring is seen close to the Galactic Plane in both tangent directions. From a practical point of view, the errors in the flow velocities are dominated by the error in p_{\odot} unless the error in z_{\odot} is larger than 3 pc. Such a large error in z_{\odot} seems unlikely.

For a constant ring radius a , we find $x_{\odot} = (52.1^{+0.7}_{-0.7})$ pc if only errors from reading the vertices are included. Let us consider the possibility that the ring radius a changes between the left and right tangent points as $a(\phi) = a_0 + a_1\phi + a_2\phi^2$ where ϕ varies from -6.3° to $+6.3^{\circ}$ between the two inner tangent directions, and $a_0 = 8.448$ kpc. When $|a_1|$ is increased, one tangent point comes closer to the Sun whereas the other moves away. We require $|a_1|$ to be less than 314.5 pc so that the distance to the nearest tangent point remains larger than half the distance in the constant radius case. Furthermore we assume that the second order coefficient $|a_2| \lesssim |a_1|/2$. Then, x_{\odot} is found to range between 43.5 and 51.6 pc, and the value of p_{\odot} between 58.2 and 94.9 pc including the uncertainty discussed in the paragraph before last.

We find that the Sun is almost certainly within the tricusp volume of the caustic ring. Given $x_{\odot} < p_{\odot}$, whether the Sun is inside or outside the tricusp is determined by its vertical distance z_{\odot} from the caustic ring plane. For the central values of x_{\odot}, p_{\odot} and q_{\odot} , the Sun is outside the tricusp if $z_{\odot} \geq 7.0$ pc which is very unlikely according to our estimates. However, the Sun is outside the tricusp for some extreme values of the parameters, e.g. $p_{\odot} = 58.2$ pc, $x_{\odot} = 52.8$ pc, $z_{\odot} = 1.3$ pc and all plausible values q_{\odot} . We estimate the probability that the Sun is outside the tricusp to be less than 1%. Assuming the Sun is indeed inside the tricusp, there are four prominent flows on Earth associated with the nearby caustic ring. In Fig. 11, for various values of z_{\odot} , we show the directions of the flows with respect to the LSR in the $\eta_0 < 0$ case and indicate their densities by the sizes of circles. As the Sun moves closer to the boundary of the tricusp, two flows approach each other in velocity space while their densities increase. They disappear the moment the Sun passes outside the tricusp.

C. Big Flow velocity vector and density estimates

The flow velocities in the frame of the caustic ring are calculated using Eqs. (2.6) and (2.8). The caustic ring parameters near the location of the Sun are derived from the central

values of a , p_\odot and q_\odot and setting $v = 520$ km/s as the speed of the flow [4]:

$$\begin{aligned}
u &= \frac{v^2 - v_{\text{rot}}^2}{a} = 26.3 \times 10^3 \text{ kpc}^{-1}(\text{km/s})^2 \\
\eta_0 &= \pm \sqrt{\frac{2p}{u}} = \pm 2.44 \times 10^{-3} \text{ kpc}(\text{km/s})^{-1} \\
\zeta &= \frac{27p^2}{16q^2} = 0.807 \quad .
\end{aligned} \tag{4.4}$$

Eqs. (2.8) give the components of the flow velocities in cylindrical coordinates attached to the caustic ring. Since the caustic ring center is displaced from the Galactic Center by $\theta = (5.80^\circ \text{ }^{+0.05^\circ}_{-0.04^\circ})$ to the right, and the caustic ring plane is tilted relative to the Galactic Plane by $\theta_t = (0.48^\circ \text{ }^{+0.20^\circ}_{-0.20^\circ})$ also to the right, the velocity components $(v_{j\rho}^G, v_{j\phi}^G, v_{jz}^G)$ of the j th flow in Galaxy centered cylindrical coordinates are obtained from the components $(v_{j\rho}, v_{j\phi}, v_{jz})$ in caustic centered cylindrical coordinates using

$$\begin{aligned}
v_{j\rho}^G &= \cos \theta v_{j\rho} - \sin \theta \cos \theta_t v_{j\phi} + \sin \theta \sin \theta_t v_{jz} \\
v_{j\phi}^G &= \sin \theta v_{j\rho} + \cos \theta \cos \theta_t v_{j\phi} - \cos \theta \sin \theta_t v_{jz} \\
v_{jz}^G &= \sin \theta_t v_{j\phi} + \cos \theta_t v_{jz}
\end{aligned} \tag{4.5}$$

where $\hat{\rho}_G$ points away from the Galactic Center, $\hat{\phi}_G$ points in the direction of Galactic Rotation and \hat{z}_G points to the Galactic North Pole. The flow velocity with respect to the LSR is $\vec{v}_{j\text{LSR}} = \vec{v}_j^G - v_{\text{rot}} \hat{\phi}_G$ with $v_{\text{rot}} = 220$ km/s. The error associated with uncertainty on v/v_{rot} enters here. It contributes of order 0.25° to the errors on the velocity directions, given in Eqs. (4.6) and (4.7) below.

Table I gives the densities d_j and velocities \vec{v}_j^G of the four flows corresponding to the central values of x_\odot , z_\odot , p_\odot and q_\odot when $\eta_0 < 0$. Table II gives the same information in case $\eta_0 > 0$. The densities are calculated using Eqs. (2.7). We set $b = v = 520$ km/s. We do not have enough information to determine b precisely but it is expected to be of order v [5]. The difference between b and v is relatively unimportant in view of the other uncertainties affecting the densities. For the infall rate, in view of the Big Vortex, we multiplied by 4 the estimate given in ref. [4], i.e. $\frac{dM}{d\Omega d\eta} = 4 \times \frac{7.8 M_\odot}{\text{sterad yr}}$. Estimates of the densities are very uncertain because the densities vary rapidly with position. Over the range of plausible parameter values, Eqs. (4.3), the Big and Up flows range from 1/2 their central values to infinity (when the Sun approaches the tricusp boundary), the Down flow ranges from 1/2 to 4 times its central value, and the Little flow changes by 20%. All entries in Tables I and II are highly correlated since they are functions of a small number of parameters, mainly x_\odot , p_\odot , q_\odot and z_\odot .

The directions of the flow velocities with respect to the LSR are:

$$\begin{aligned}
(l, b)|_{\text{Big}} &= (70.17^\circ \text{ }^{+0.84^\circ}_{-0.19^\circ}, 1.14^\circ \text{ }^{+2.09^\circ}_{-0.59^\circ}) \\
(l, b)|_{\text{Little}} &= (89.96^\circ \text{ }^{+0.07^\circ}_{-0.87^\circ}, 0.86^\circ \text{ }^{+0.38^\circ}_{-0.36^\circ}) \\
(l, b)|_{\text{Up}} &= (67.97^\circ \text{ }^{+1.91^\circ}_{-1.81^\circ}, 8.28^\circ \text{ }^{+2.44^\circ}_{-5.01^\circ}) \\
(l, b)|_{\text{Down}} &= (67.81^\circ \text{ }^{+1.72^\circ}_{-1.76^\circ}, -7.05^\circ \text{ }^{+3.58^\circ}_{-2.35^\circ}) \quad .
\end{aligned} \tag{4.6}$$

in case $\eta_0 < 0$ and

$$(l, b)|_{\text{Big}} = (89.96^\circ \text{ }^{+0.19^\circ}_{-0.87^\circ}, 0.49^\circ \text{ }^{+0.61^\circ}_{-2.15^\circ})$$

TABLE I: Central values of the densities and velocities of the flows through the Sun associated with the nearby caustic in the Galactic Rest Frame in case $\eta_0 < 0$. The densities are uncertain by a factor of 2 or more, as discussed in the text. The error on the velocity components is dominated by the uncertainty in the rotation speed of the LSR, taken to be 220 km/s but known only within approximately 10%. The velocity directions and their errors are given explicitly in Eqs. (4.6) and Fig. 12.

Flow	d [10^{-24} g/cm 3]	v_ρ^G [km/s]	v_ϕ^G [km/s]	v_z^G [km/s]
Big	20.0	-104.4	509.4	6.1
Little	2.0	-0.2	520.0	4.5
Up	9.6	-115.3	505.1	44.8
Down	8.4	-116.4	505.4	-38.1

TABLE II: Same as Table I but for $\eta_0 > 0$. The velocity directions and their errors are given explicitly in Eqs. (4.7) and Fig. 13.

Flow	d [10^{-24} g/cm 3]	v_ρ^G [km/s]	v_ϕ^G [km/s]	v_z^G [km/s]
Big	20.0	-0.2	520.0	2.7
Little	2.0	-104.4	509.4	4.4
Up	8.4	12.7	517.7	47.1
Down	9.6	11.5	518.6	-35.8

$$\begin{aligned}
(l, b)|_{\text{Little}} &= (70.17^\circ \begin{smallmatrix} +0.84^\circ \\ -0.06^\circ \end{smallmatrix}, 0.77^\circ \begin{smallmatrix} +0.36^\circ \\ -0.36^\circ \end{smallmatrix}) \\
(l, b)|_{\text{Up}} &= (92.40^\circ \begin{smallmatrix} +1.82^\circ \\ -1.78^\circ \end{smallmatrix}, 8.91^\circ \begin{smallmatrix} +2.43^\circ \\ -3.69^\circ \end{smallmatrix}) \\
(l, b)|_{\text{Down}} &= (92.18^\circ \begin{smallmatrix} +1.85^\circ \\ -1.93^\circ \end{smallmatrix}, -6.90^\circ \begin{smallmatrix} +5.20^\circ \\ -2.52^\circ \end{smallmatrix}).
\end{aligned} \tag{4.7}$$

in case $\eta_0 > 0$. The directions and errors are displayed in Figs. 12 and 13 for $\eta_0 < 0$ and $\eta_0 > 0$ respectively. To obtain the flow velocities with respect to an observer on Earth, one needs to subtract from the velocities given in Tables I and II the velocity of the Sun with respect to the LSR and the velocity of the observer with respect to the Sun due to the orbital and rotational motions of the Earth.

V. SUMMARY

In this paper we added to the observational evidence in support of caustic rings and the Caustic Ring Model. The additional evidence is found in the rotation curve of our closest large Galactic Neighbor M31 [36] and in a triangular feature in the Gaia map [21, 22] of the Milky Way in the direction of Galactic Coordinates $(l, b) = (-91^\circ, 0^\circ)$. The M31 rotation curve has bumps whose locations are in rough agreement with the model predictions for the radii of the first three ($n = 1, 2, 3$) caustic rings. The bumps attributed to the $n = 1$ ring are particularly striking as they appear at the same location on both the receding and approaching sides of the rotation curve, strongly suggesting the existence of a ring structure in the M31 halo with a diameter of order 60 kpc.

The Gaia triangular feature at $(l, b) = (-91^\circ, 0^\circ)$ solves a question raised by a previous claim [20] that a triangular feature in the IRAS map, in the direction $(l, b) = (80^\circ, 0^\circ)$, is

the imprint of the 5th caustic ring ($n = 5$) on baryonic matter in the Galactic Disk, seen in a tangent direction to the caustic ring from our viewpoint. The 5th caustic ring has two tangent directions from our viewpoint, and there is no triangular feature in the IRAS map on the opposite side, near $(l, b) = (-80^\circ, 0^\circ)$. In contrast, the Gaia map has two triangular features at nearly symmetrical locations, one which coincides with the IRAS feature on the left side, and the new feature on the right side. The triangular feature on the right side, like the one on the left, is to a high level of accuracy an isosceles triangle with axis parallel to the Galactic Plane. It has approximately the same aspect ratio as the left triangle but is 40% smaller. It was emphasized earlier [6] that the transverse size of a caustic ring cross-section may vary along the ring.

The Gaia triangles are features in the distribution of dust. Like the IRAS triangle, they are much sharper than they would be if produced by gas and dust in thermal equilibrium in the gravitational field of the caustic ring [23]. We propose here instead that dust is entrained by the axion flows forming the 5th caustic ring. By following the same trajectories as the axions, the dust particles form the same caustics. This would explain the sharpness of the features. Section III discusses the entrainment of a dust particle by a cold axion flow. The axions in the flow are assumed to be a highly degenerate Bose gas at temperature T , with almost all axions therefore in a single state forming a Bose-Einstein condensate. We derived a formula, Eq. (3.13), for the frictional deceleration of a dust particle moving with respect to the cold axion flow. The deceleration is proportional to T^{-1} . We estimate the temperature cold dark matter axions have today taking account of the heat in the axions themselves and of heat they absorb by cooling baryons. Our formula for friction indicates that the dust particle is efficiently entrained by the axion flow. However, in the Galactic Disk collisions with gas may slow down the dust particle considerably. On the other hand the collisions with gas do not diffuse the flow of dust particles. We conjecture that the dust particles, although slowed down by collisions with gas in the disk, follow the same trajectories as the axions and form the same caustics.

We also proposed an explanation why the features seen in the IRAS and Gaia maps are triangular even though the cross-section of a caustic ring is tricusp. For accepted values of the dust density and dust grain size, the flow of dust inside the caustic ring is collisionless but only barely so. The density in the three flows forming the cusps of a tricusp is much higher than elsewhere within the tricusp. Dust-dust collisions within the cusps are likely to fuzz them up. The observed features are then qualitatively triangles inscribed in the tricusp, as indicated in Fig. 10. Finally, we proposed an explanation why no right triangle is seen in the IRAS map. IRAS observes in the infra-red. Dust particles emit in the infrared when heated by stellar radiation. In the left tangent direction, the 5th caustic ring lies in the midst of a spiral arm with abundant stellar activity whereas in the right tangent direction, the ring lies in a quiet region. The dust on the right sides receives less heat and for this reason fails to show up in the IRAS map.

The GAIA and IRAS triangular features imply that the caustic ring center is displaced from the Galactic Center to the right by 5.8° , and that the plane of the ring is tilted relative to the Galactic Plane 0.48° to the right. In all likelihood, we on Earth are inside the tricusp volume of the nearby caustic ring. As a result there are four flows on Earth associated with the nearby caustic, called Big, Little, Up and Down. In contrast, on the basis of pre-Gaia observations when only the IRAS triangle was known and the caustic ring center was assumed to coincide with the Galactic Center, it was thought that we are outside the tricusp and hence that there are two flows on Earth associated with the nearby caustic, Big and

Little. Being inside the tricusp implies two additional flows, Up and Down.

The flows that form the 5th caustic ring are prominent on Earth. They produce narrow peaks in the axion energy spectrum which are observable with great resolution in the cavity haloscopes [50]. These detectors are made more sensitive by searching for such narrow peaks [52]. Knowing the velocity vectors of the flows on Earth one can calculate how the peaks move as a function of time of day and time of year [53], so that observations made at different times can be related to one another. Generally speaking, axion dark matter searches are helped by knowing the velocity distribution of the axions on Earth. In particular, a recently proposed axion dark matter detection scheme [51], called the axion echo method, is largely predicated on the existence of one or more cold flows and on knowledge of their velocity vectors. So there is strong motivation to determine the velocity vectors on Earth of the flows forming the nearby caustic ring. This is our purpose in Section IV. Even accepting that the IRAS and Gaia triangles show the imprints of the 5th caustic ring in the two tangent directions, uncertainties arise because of the need to interpolate between the two tangent points, which are 940 pc away from us on either side. To find the central values of the flow velocity vectors we assume that the ring between the two tangent points is planar and circular. We also assume that the caustic ring transverse sizes at our location, p and q , can be obtained from estimates at the tangent points by linear interpolation. We estimate the likely errors associated with these assumptions. The results are given in Eqs. (4.6) and (4.7), Tables I and II, and Figs. 12 and 13. These predictions are testable as soon as axion dark matter is detected in the laboratory, and perhaps by other means.

Acknowledgments

We gratefully acknowledge stimulating discussions with Peter Barnes, David Tanner, Shriram Sadashivajois, Ariel Arza and Richard Bradley. This work was supported in part by the U.S. Department of Energy under grant DE-SC0010296 at the University of Florida. SSC is supported by the grant “The Milky Way and Dwarf Weights with Space Scales” funded by University of Torino and Compagnia di S. Paolo (UniTO-CSP). SSC also acknowledges partial support from the INFN grant InDark and the Italian Ministry of Education, University and Research (MIUR) under the Departments of Excellence grant L.232/2016.

Appendix A: Statistical significance of the Gaia left and right triangles

The Gaia skymap is a greyscale map of the logarithm $g(l, b)$ of the number of stars per unit solid angle [22] observed by the Gaia satellite in the direction of Galactic Coordinates (l, b) . We obtained $g(l, b)$ from the Gaia data archive [40] over a grid of spacing $\delta l = \delta b = 0.1^\circ$ covering the range $-180^\circ < l < 180^\circ$ and $-5^\circ < b < 5^\circ$. We made a cut on the distances from Earth to the stars in the Gaia catalog since the signal is due only to stars that are behind the caustic ring tangent points, approximately 1 kpc away. We only used sources that are more than 0.8 kpc away from Earth.

First, we convoluted the map with a square top hat filter of size $\Delta l = \Delta b = 5^\circ$ placed at $72 = 360/5$ successive adjacent positions along the Galactic Plane. For each position, we calculated the average value \bar{g}_i ($i = 1, 2, \dots, 72$) of $g(l, b)$ within the rectangle at that position, and the deviation $\Delta\bar{g}_i$ of \bar{g}_i from its average over the n neighboring positions to the left plus the n neighboring positions to the right, where $n = 5, 3$ and 2 . Changing the value of n

did not change the final results significantly. The results reported here are for $n = 5$. The three largest negative fluctuations in $\Delta\bar{g}_i$ are at the positions of the right ($l \simeq -91^\circ$) and left ($l \simeq 80^\circ$) triangles and at a relatively dark area in the Gaia skymap near ($b \simeq 0, l \simeq 37^\circ$). These three largest negative fluctuations are respectively -2.5σ , -3.8σ and -2.6σ where σ is the root mean square of all the $\Delta\bar{g}_i$. Indeed, looking by eye, the darkest areas along the Galactic Plane are seen at those three locations in the Gaia skymap. The dark area at $l \simeq 37^\circ$ is somewhat triangular in shape, pointing to the left like the left triangle. Its position is consistent with that of a prominent rise in the inner Galactic Rotation Curve derived from the Massachusetts-Stony Brook North Galactic Plane CO Survey [31] between 35.3° and 38.7° and attributed to the 9th caustic ring in the Caustic Ring Model of the Milky Way halo [20]. As the 9th caustic ring is not the topic of this paper, we do not discuss the dark area near $l \simeq 37^\circ$ further. We remove it from the data so that it is counted neither as signal nor as noise.

Second, we convoluted the map with a triangular top hat filter whose size and Galactic Latitude matches that of the right triangle in the Gaia skymap. It is isosceles, parallel to the Galactic Plane, pointing to the right, with height $\Delta b = 3.6^\circ$, width $\Delta l = 3.5^\circ$ and displaced 0.5° below the Galactic Plane. These properties are consistent with the positions of the vertices of the right triangle stated in Section 4.B. The filter is moved to the left and right and the average $\bar{g}(l)$ of $g(l, b)$ over the area of the filter is calculated for each position l . We then fit $\bar{g}(l)$ with a second order polynomial in l after removing the regions $(73^\circ, 85^\circ)$, $(33^\circ, 45^\circ)$, and $(-95^\circ, -85^\circ)$ which contain the features attributed to caustic rings. We also exclude $(-75^\circ, -45^\circ)$ as it is along the direction of a major spiral arm of the Milky Way. The deviation $\Delta\bar{g} \equiv \bar{g} - \bar{g}_{\text{fitted}}$ from the fitted curve is -5.1σ where σ is the root mean square of all $\Delta\bar{g}$ other than those in the excluded regions. This is illustrated in the top panel of Fig. 14.

Finally, we convoluted the map with a triangular top hat filter whose size and Galactic Latitude matches that of the left triangle in the Gaia skymap. It is isosceles, parallel to the Galactic Plane, pointing to the left, with height $\Delta b = 5.7^\circ$, width $\Delta l = 5.2^\circ$ and displaced 0.4° above the Galactic Plane. These properties are consistent with the positions of the vertices of the left triangle stated in Section 4.B. The analysis is similar to that using the right triangle top hat filter. The filter is moved to the left and right and the average $\bar{g}(l)$ of $g(l, b)$ over the area of the filter is calculated for each position l . $\bar{g}(l)$ is fitted with a second order polynomial in l after exclusion of the same regions as stated above. The deviation $\Delta\bar{g} \equiv \bar{g} - \bar{g}_{\text{fitted}}$ at the position of the left triangle is $-6.5\sigma'$ where σ' is the root mean square of all $\Delta\bar{g}$ other than those in the excluded regions. This is illustrated in the bottom panel of Fig. 14.

-
- [1] Reviews include: *Particle Dark Matter* edited by Gianfranco Bertone, Cambridge University Press 2010; E.W. Kolb and M. Turner, *The Early Universe*, Addison Wesley 1990.
- [2] P. Sikivie and J.R. Ipser, Phys. Lett. B291 (1992) 288.
- [3] A. Natarajan and P. Sikivie, Phys. Rev. D72 (2005) 083513.
- [4] L.D. Duffy and P. Sikivie, Phys. Rev. D78 (2008) 063508.
- [5] P. Sikivie, Phys. Rev. D60 (1999) 063501.
- [6] A. Natarajan and P. Sikivie, Phys. Rev. D73 (2006) 023510.
- [7] R. D. Peccei and H. Quinn, Phys. Rev. Lett. **38** (1977) 1440 and Phys.Rev. **D16** (1977) 1791; S. Weinberg, Phys. Rev. Lett. **40** (1978) 223; F. Wilczek, Phys. Rev. Lett. **40** (1978) 279.
- [8] J. Kim, Phys. Rev. Lett. **43** (1979) 103; M. A. Shifman, A. I. Vainshtein and V. I. Zakharov, Nucl. Phys. **B166** (1980) 493; M. Dine, W. Fischler and M. Srednicki, Phys. Lett. **B104** (1981) 199; A. Zhitnitskii, Sov. J. Nucl. 31 (1980) 260.
- [9] P. Arias et al., JCAP 06 (2012) 013.
- [10] J. Preskill, M. Wise and F. Wilczek, Phys. Lett. **B120** (1983) 127; L. Abbott and P. Sikivie, Phys. Lett. **B120** (1983) 133; M. Dine and W. Fischler, Phys. Lett. **B120** (1983) 137.
- [11] P. Sikivie and Q. Yang, Phys. Rev. Lett. 103 (2009) 111301
- [12] O. Erken, P. Sikivie, H. Tam and Q. Yang, Phys. Rev. D85 (2012) 063520.
- [13] N. Banik, A.J. Christopherson, P. Sikivie and E.M. Todarello, Phys. Rev. D95 (2017) 043542.
- [14] N. Banik and P. Sikivie, Phys. Rev. D88 (2013) 123517.
- [15] P. Sikivie, Phys. Lett. B695 (2011) 22.
- [16] S. Davidson and M. Elmer, JCAP 1312 (2013) 034.
- [17] S. Davidson, Astropart. Phys. 65 (2015) 101.
- [18] A.H. Guth, M.P. Hertzberg and C. Prescod-Weinstein, Phys. Rev. D92 (2015) 103513.
- [19] S.S. Chakrabarty et al., Phys. Rev. D97 (2018) 043531.
- [20] P. Sikivie, Phys. Lett. B567 (2003) 1.
- [21] A.G.A. Brown et al. (the Gaia Collaboration), Astron. Astrophys. 595 (2016) A2.
- [22] A.G.A. Brown et al. (the Gaia Collaboration), Astron. Astrophys. 616 (2018) A1.
- [23] S.S. Chakrabarty and P. Sikivie, Phys. Rev. D98 (2018) 103009.
- [24] P.J.E. Peebles, Ap. J. 155 (1969) 393.
- [25] J.A. Fillmore and P. Goldreich, Ap. J. 281 (1984) 1; E. Bertschinger, Ap. J. Suppl. 58 (1985) 39.
- [26] P. Sikivie, I. Tkachev and Y. Wang, Phys. Rev. Lett. 75 (1995) 2911; Phys. Rev. D56 (1997) 1863.
- [27] P. Sikivie, Phys. Lett. B432 (1998) 139.
- [28] K.G. Begeman, A.H. Broeils and R.H. Sanders, MNRAS 249 (1991) 523; R.H. Sanders, Ap. J. 473 (1996) 117.
- [29] W.H. Kinney and P. Sikivie, Phys. Rev. D61 (2000) 087305.
- [30] D.P. Clemens, Ap. J. 569 (1985) 422.
- [31] D.B. Sanders et al., Ap. J. Suppl. 60 (1986) 1; D.P. Clemens et al., Ap. J. Suppl. 60 (1886) 297.
- [32] R.P. Olling and M.R. Merrifield, MNRAS 311 (2000) 361.
- [33] J. Binney and W. Dehnen, MNRAS 287 (1997) L5.
- [34] H.J. Newberg et al. (the SDSS Collaboration), Ap. J. 569 (2002) 245; B. Yanny et al. (the

- SDSS Collaboration), Ap. J. 588 (2003) 824 [Erratum: Ap. J. 605 (2004) 575]; R.A. Ibata et al., MNRAS 340 (2003) L21.
- [35] A. Natarajan and P. Sikivie, Phys. Rev. D76 (2007) 023505.
 - [36] L. Chemin, C. Carignan and T. Foster, Ap. J. 705 (2009) 1395.
 - [37] Y. Sofue, Pub. Astron. Soc. Japan 67 (2015) 75.
 - [38] G.M. Green et al., Ap. J. 887 (2019) 1.
 - [39] G.M. Green et al., Mon. Not. Roy. Astron. Soc.478 (2018) 651.
 - [40] <https://sci.esa.int/web/gaia> .
 - [41] S. Chandrasekhar, Ap. J. 97 (1943) 255.
 - [42] J. Binney and S. Tremaine, *Galactic Dynamics*, Princeton University Press 1987.
 - [43] J. Berges and J. Jaeckel, Phys. Rev. D91 (2015) 025020.
 - [44] O. Erken, P. Sikivie, H. Tam and Q. Yang, Phys. Rev. Lett. 108 (2012) 061304.
 - [45] N. Aghanim et al. (the Planck Collaboration), arXiv:1807.06209.
 - [46] J.D. Bowman et al., Nature 555 (2018) 67.
 - [47] P. Sikivie, Phys. Dark Univ. 24 (2019) 100289.
 - [48] N. Houston et al., Phys. Rev. Lett. 121 (2018) 111301.
 - [49] B.T. Draine, Ann. Rev. Astron. & Astroph. 41 (2003) 241.
 - [50] T. Braine et al., Phys. Rev. Lett. 124 (2020) 10; B.M. Brubaker et al., Phys. Rev. Lett. 118 (2017) 061302; S. Lee et al., arXiv:2001.05102; D. Alesini et al., Phys. Rev. D99 (2019) 101101 (R); B.T. McAllister et al., Phys. Dark Univ. 18 (2017) 67; A. Alvarez Melcon et al., JCAP 05 (2018) 040.
 - [51] A. Arza and P. Sikivie, Phys. Rev. Lett. 123 (2019) 131804.
 - [52] L. Duffy et al., Phys. Rev. Lett. 95 (2005) 091304, and Phys. Rev. D74 (2006) 012006.
 - [53] F.-S. Ling, P. Sikivie and S. Wick, Phys. Rev. D70 (2004) 123503.

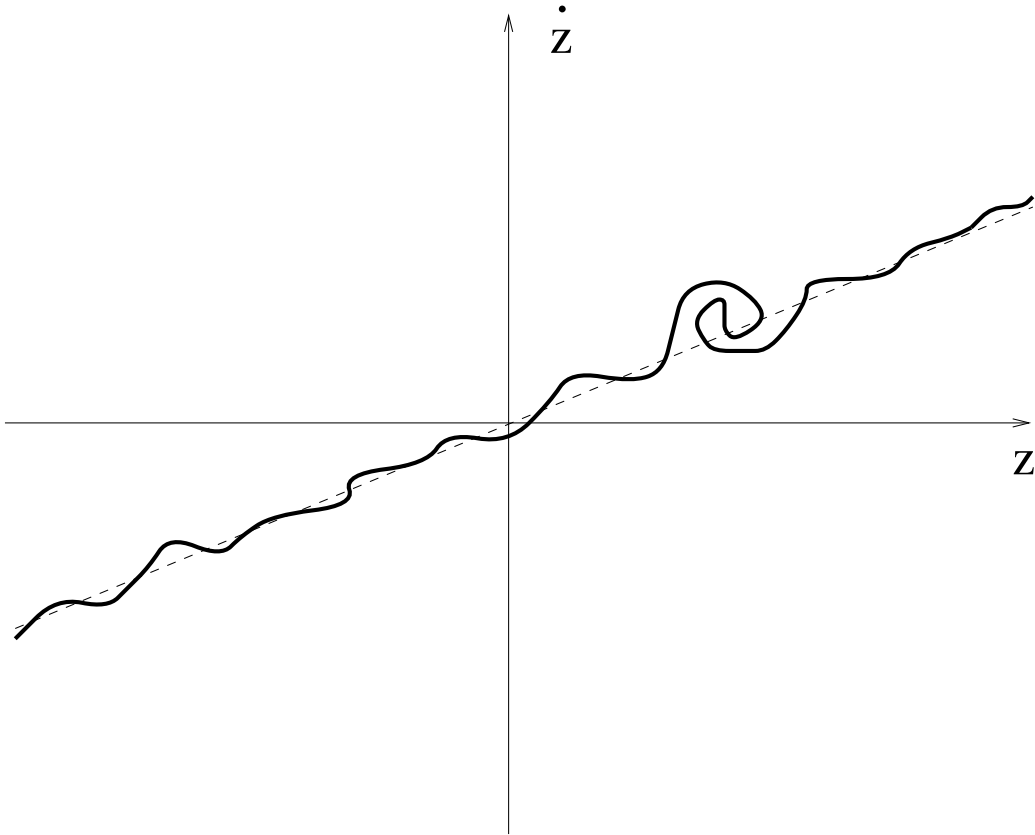


FIG. 1: Illustration of the behaviour of the 3-dimensional hypersurface, called the phase-space sheet, on which cold collisionless dark matter particles lie in 6-dimensional phase-space. The wiggly line is the intersection of the phase-space sheet with the (z, \dot{z}) plane. The thickness of the line is the primordial velocity dispersion. The broad slope of the line is the Hubble-Lemaitre expansion rate. The wiggle amplitudes are the local peculiar velocities. Where an overdensity grows in the non-linear regime, the line winds up in clockwise fashion. One such overdensity is shown. The figure is taken from ref. [5]. Reproduced with permission of the journal.

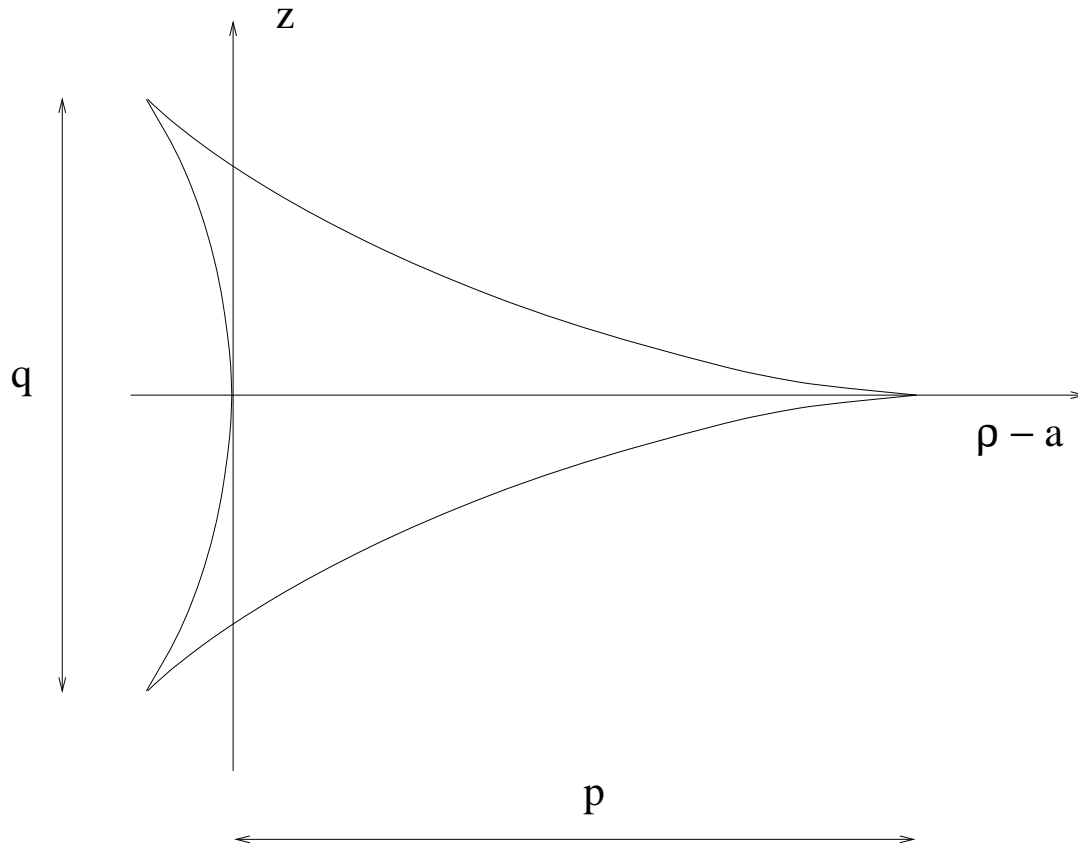


FIG. 2: The tricuspid cross-section of a caustic ring on the ρ - z plane. The dimensions of the tricuspid in the radial and vertical directions are called p and q , respectively. The figure is taken from ref. [5]. Reproduced with permission of the journal.

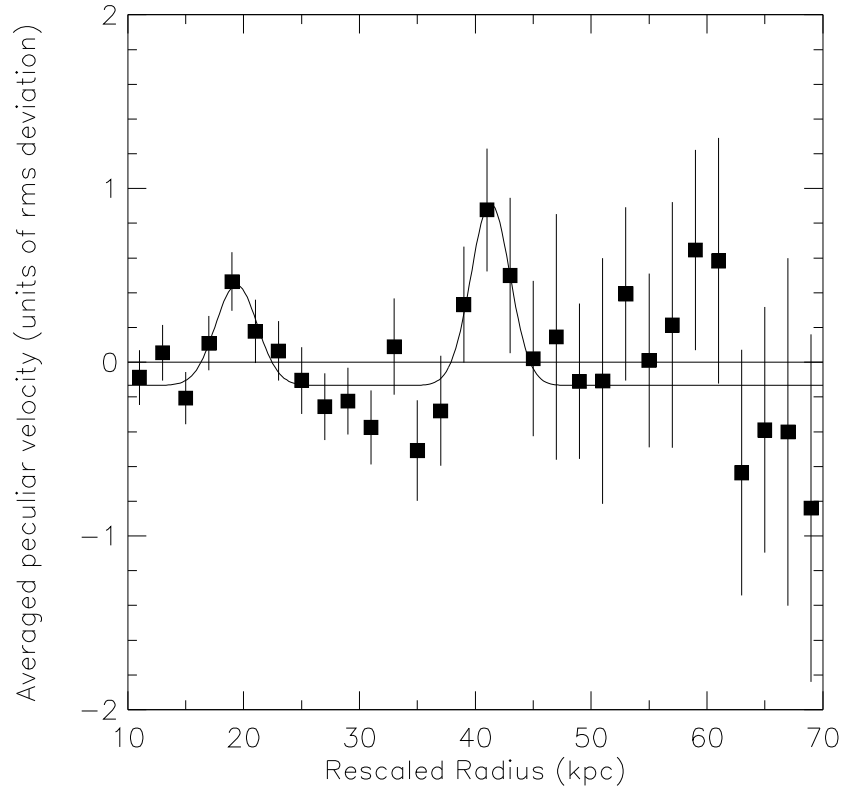


FIG. 3: Combined rotation curve of a sample of 32 galaxies, as described in the text. The figure is taken from ref. [29]. Reproduced with permission of the journal.

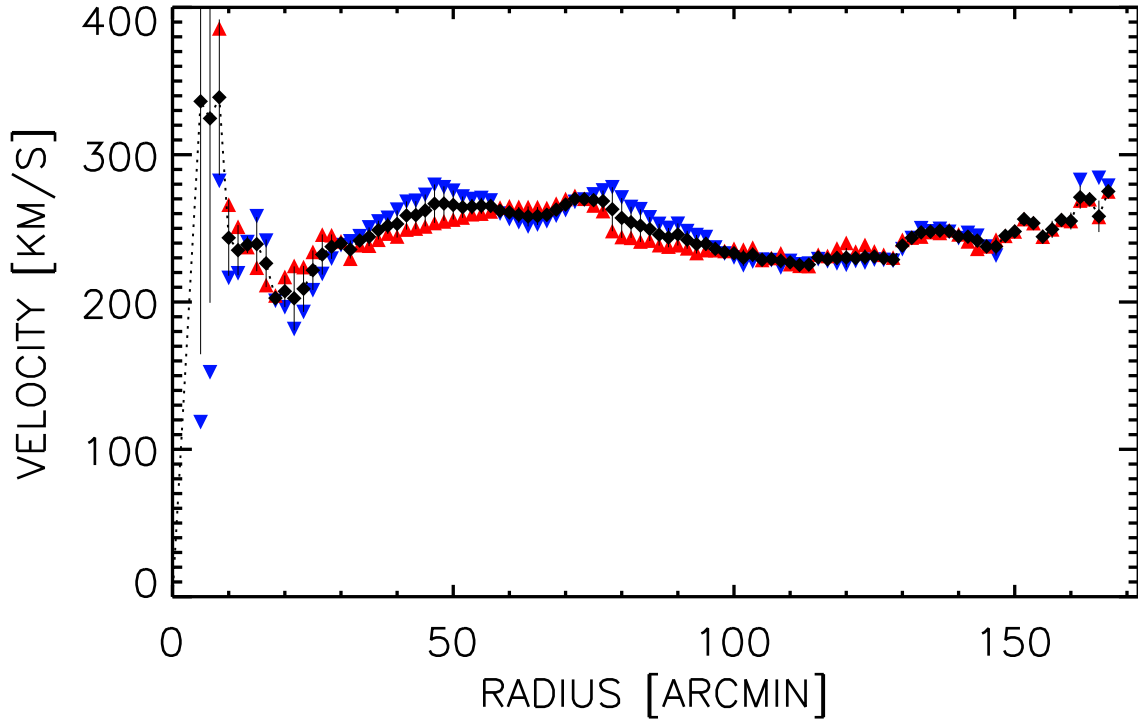


FIG. 4: Rotation curve of M31 obtained by L. Chemin, C. Carignan and T. Foster [36]. Filled diamonds are for both halves of the disc fitted simultaneously while blue downward/red upward triangles are for the approaching/receding sides fitted separately. The bumps mentioned in the text are near 135 arcmin = 30.9 kpc, 70 arcmin = 16 kpc , and 47 arcmin = 10.8 kpc. Reproduced with permission from the journal.

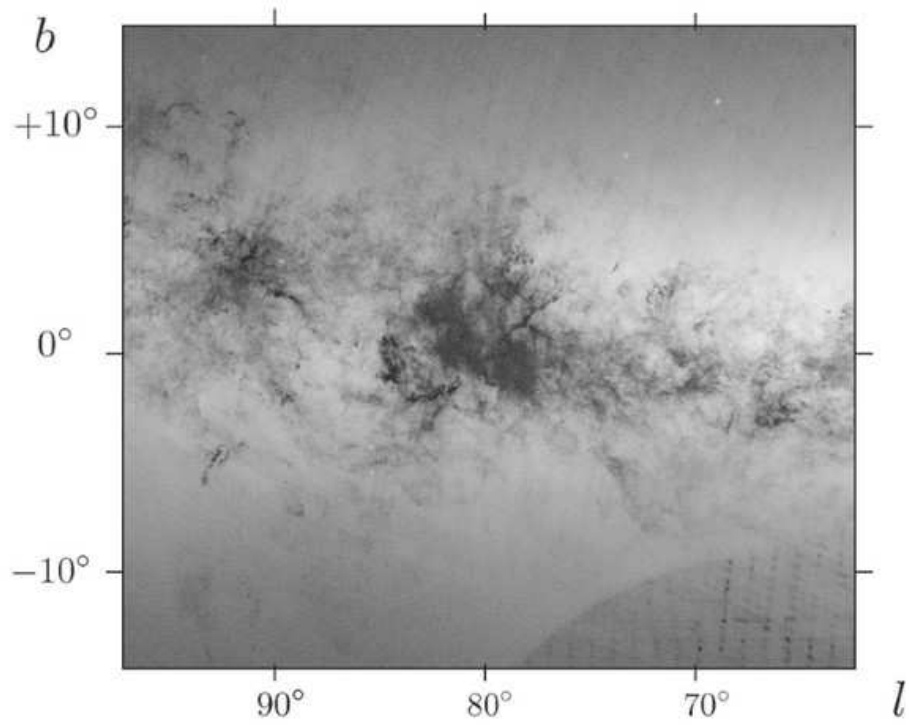


FIG. 5: Part of the Gaia skymap of the Galactic Plane with the left triangular feature at the center.

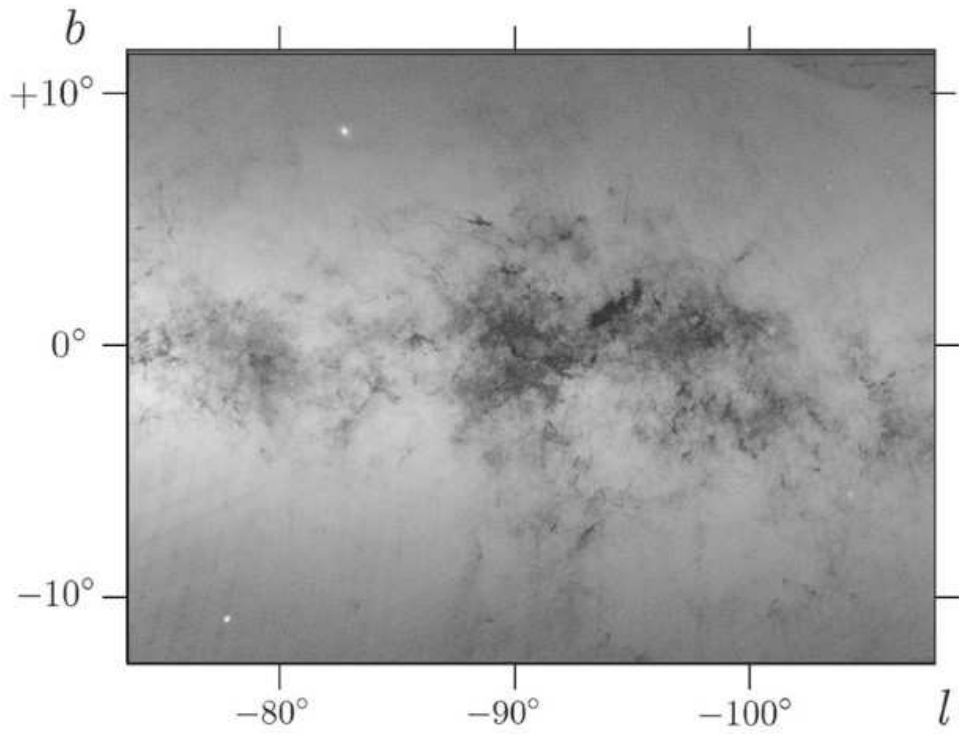


FIG. 6: Part of the Gaia skymap of the Galactic Plane with the right triangular feature at the center.

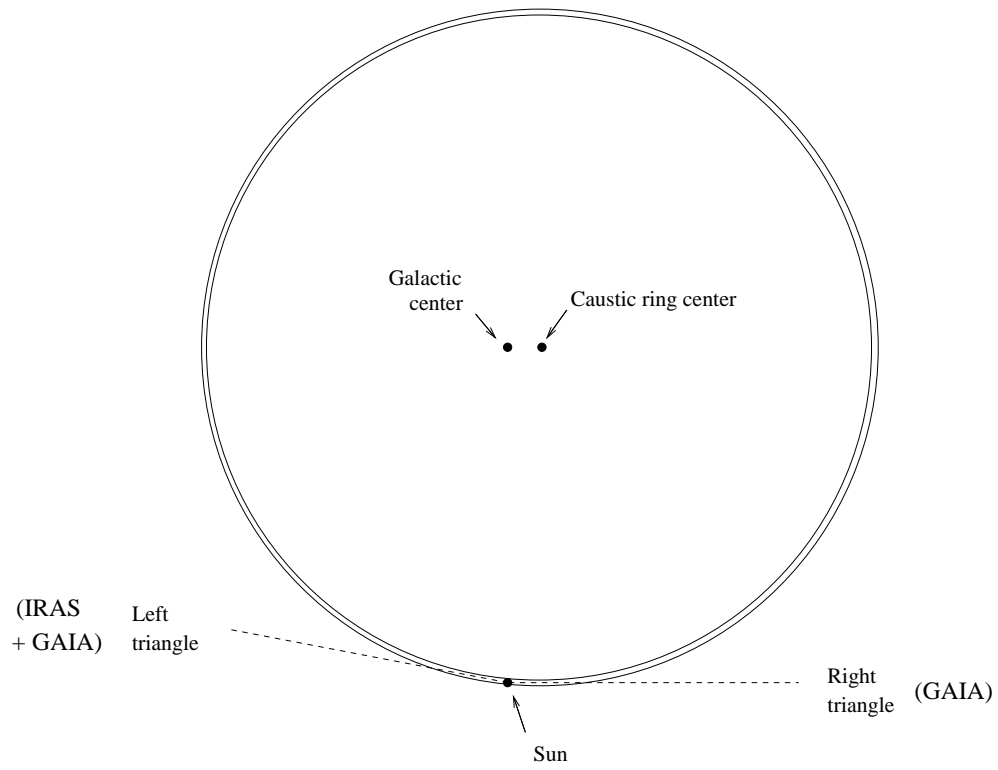


FIG. 7: Illustration of the relative positions of the Sun, caustic ring center and Galactic Center. It relies on a number of idealizations. How circular the ring is is not known. Near the Sun the actual ring is narrower than shown, and its width varies along its circumference. Only the direction of the caustic ring center relative to the Sun is known from observation.

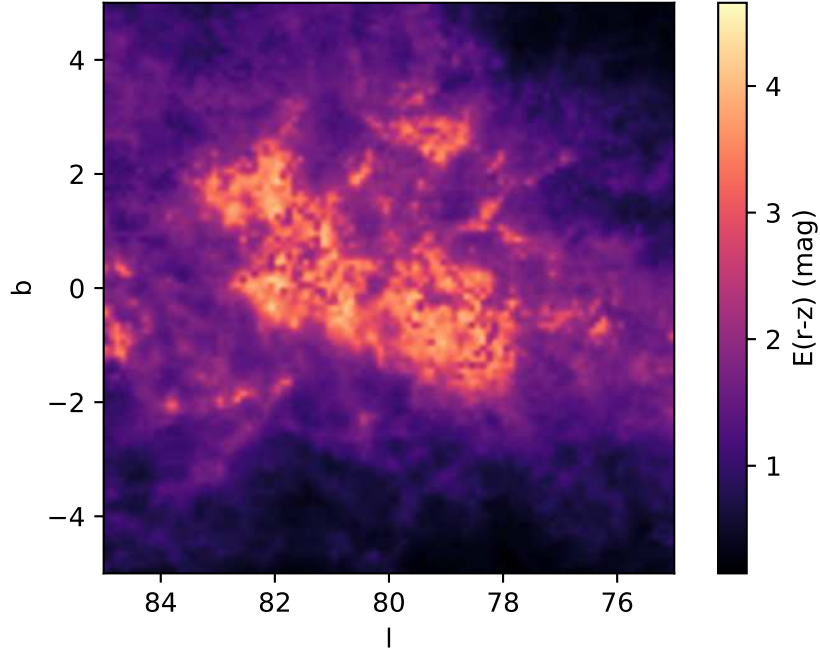


FIG. 8: Accumulated reddening from dust at $(l, b) = (80^\circ, 0^\circ)$, up to 3.5 kpc. [39]

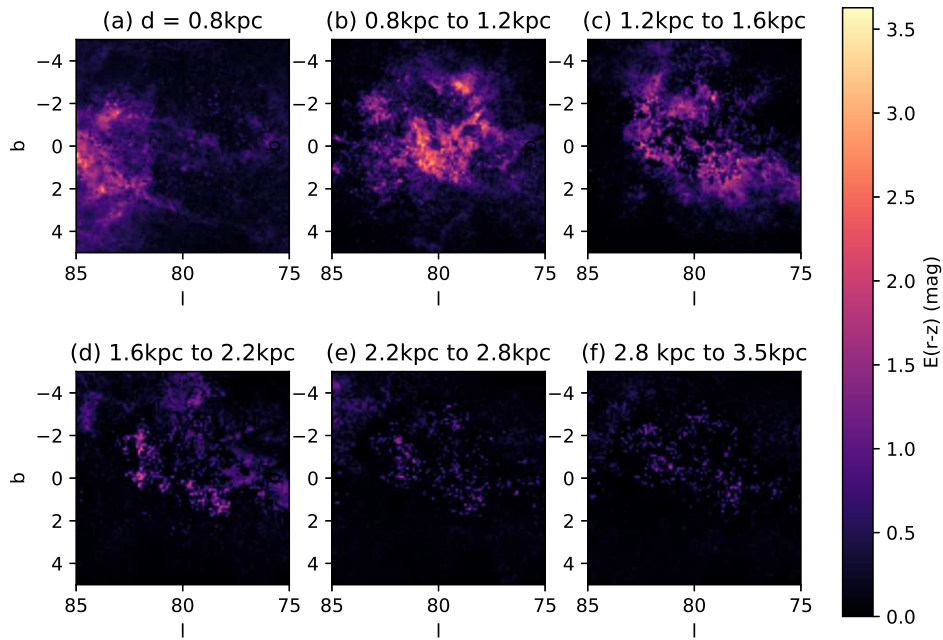


FIG. 9: Accumulated reddening from successive distance slices at $(l, b) = (80^\circ, 0^\circ)$. The color bar has been rescaled to enhance the contrast.

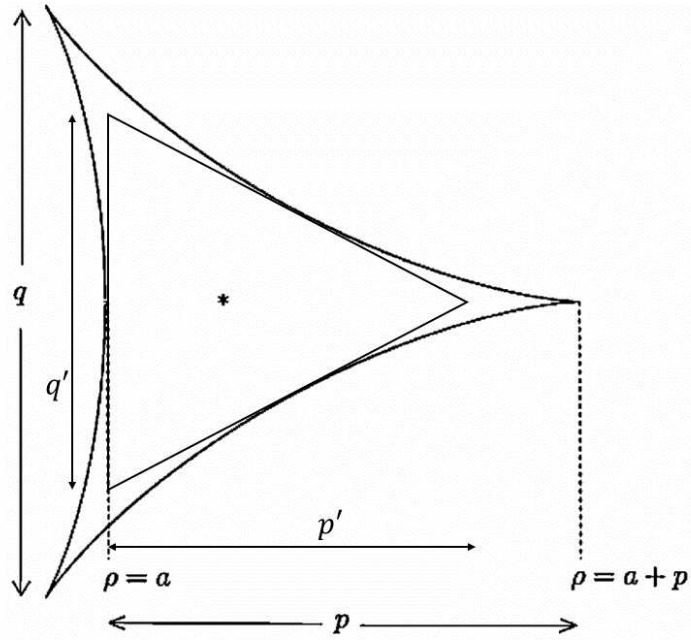


FIG. 10: Triangle inscribed in a tricuspid. We assume that the observed triangles are in the direction of the triangles inscribed in the 5th caustic ring tricuspid. The horizontal and vertical sizes of a tricuspid are related to those of the inscribed triangle by: $p = \frac{4}{3}p'$ and $q = \frac{3}{2}q'$.

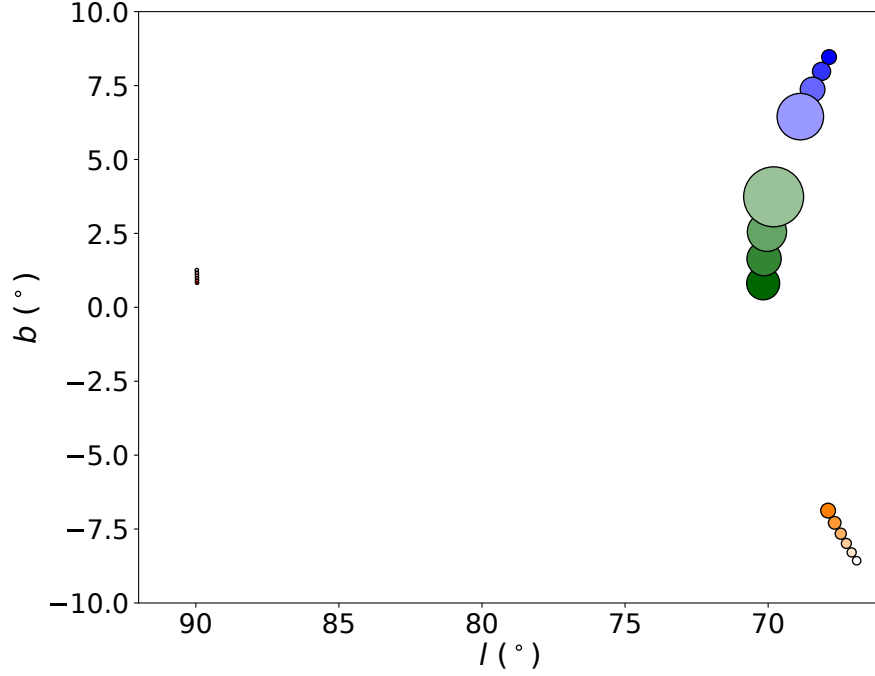


FIG. 11: Galactic Coordinates of the directions of the four flows associated with the nearby caustic ring, at the Sun, with respect to the LSR, in case $\eta_0 < 0$, for values of the vertical coordinate of the Sun $z_{\odot} = 0, 2, 4, 6, 8, 10$ pc. The sizes of the circles are proportional to the corresponding flow densities. The transparency of the circles increases with increasing z_{\odot} . There are four flows through the Sun when it is inside the tricusp. As the Sun approaches the tricusp boundary, two of the flows move towards each other in velocity space and their densities increase. When z_{\odot} changes from 6 to 8 pc, the Sun moves outside the tricusp and those two flows disappear.

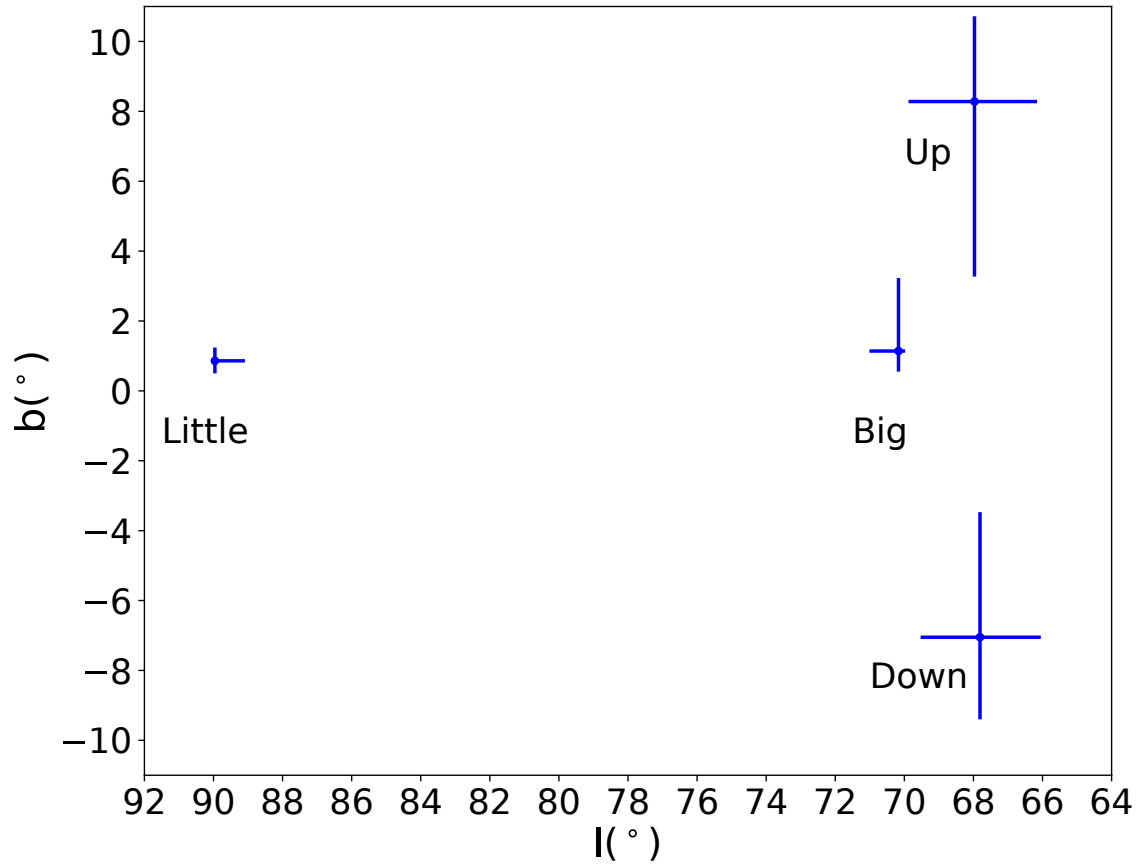


FIG. 12: Galactic Coordinates of the directions of the four flows associated with the nearby caustic ring, at the Sun, with respect to the LSR when $\eta_0 < 0$. The error bars express the uncertainties in our estimates.

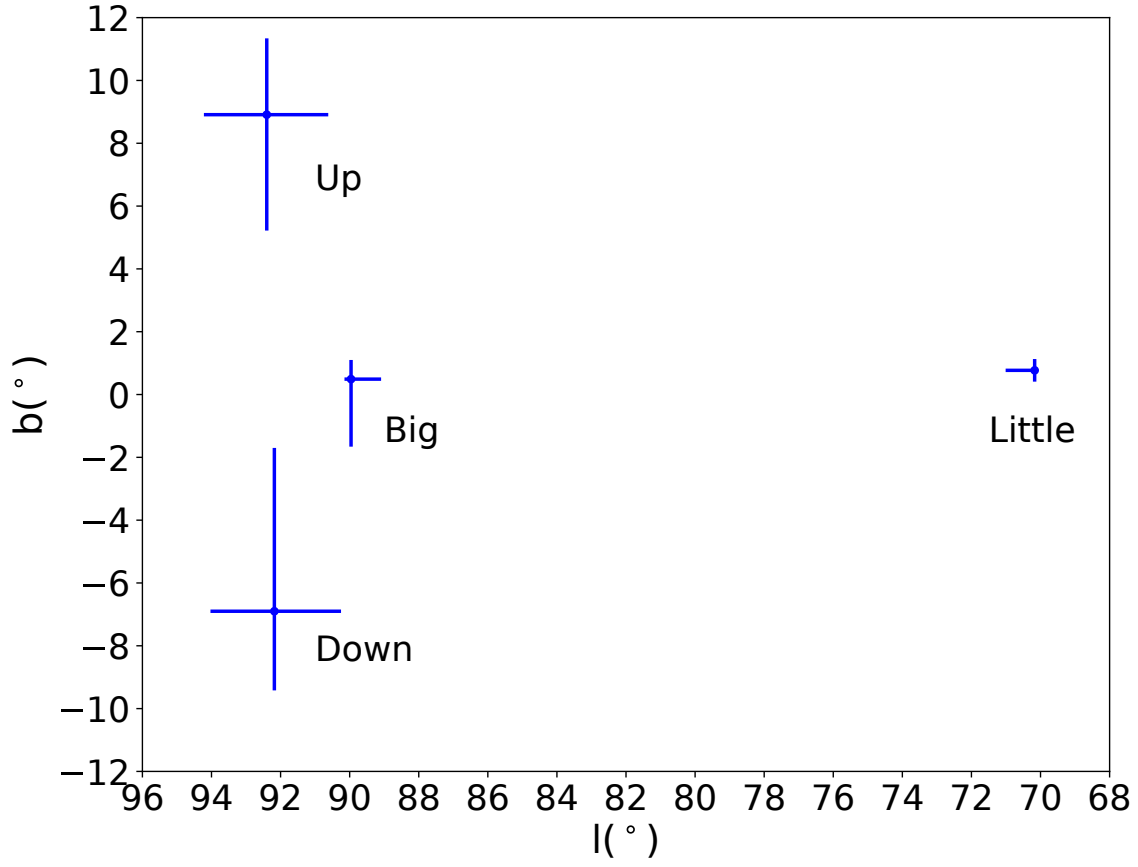


FIG. 13: Galactic Coordinates of the directions of the four flows associated with the nearby caustic ring, at the Sun, with respect to the LSR when $\eta_0 > 0$. The error bars express the uncertainties in our estimates.

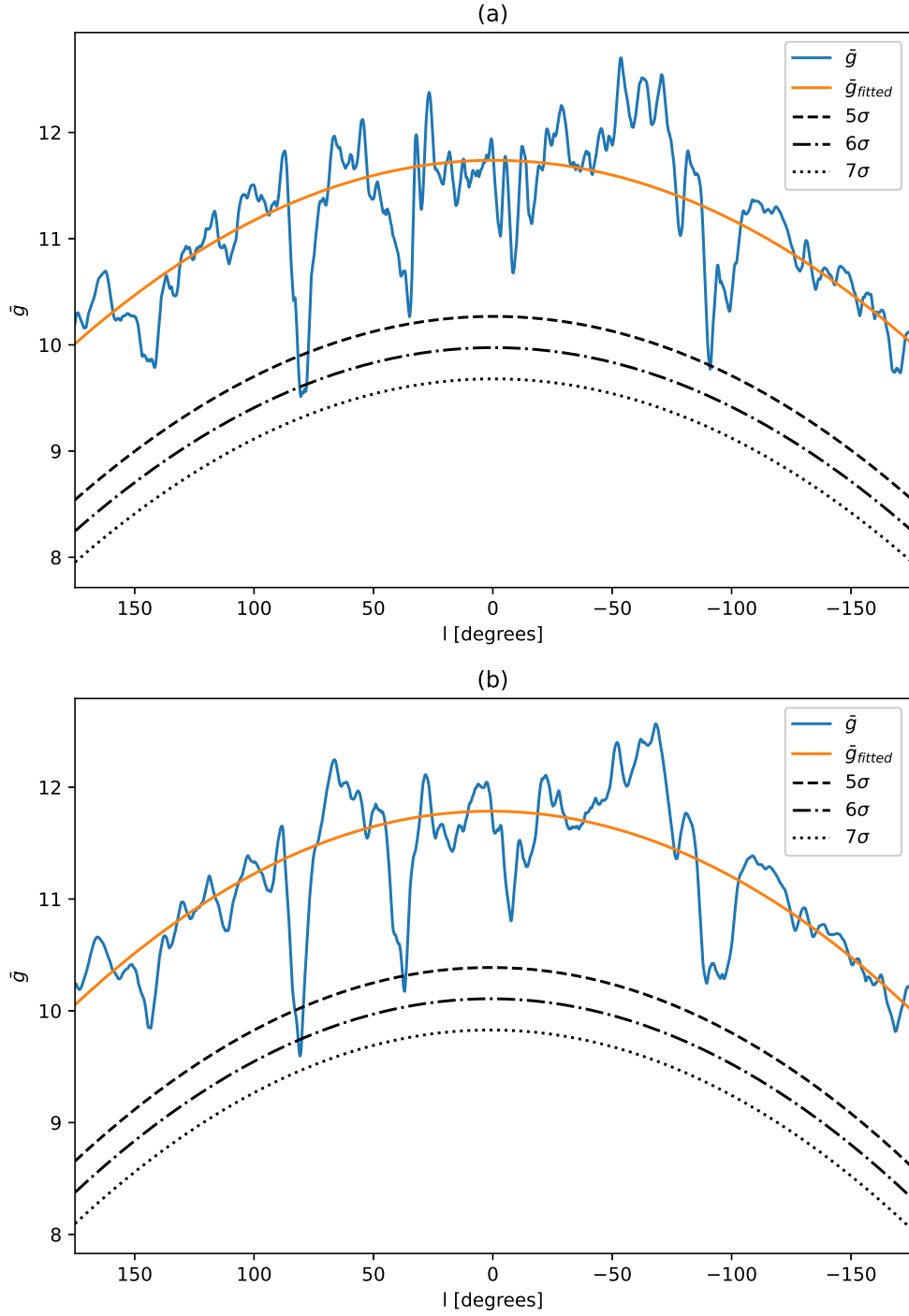


FIG. 14: (a) Convolution of the logarithm of the number of stars per square degree in the direction of Galactic Coordinates (l, b) with a triangular top hat filter matching the right triangle in the Gaia skymap but displaced in the equatorial direction by an arbitrary amount, as a function of its position l . (b) Same as in (a) but for the left triangle.